Annual Letter Report

OFFICE OF NAVAL RESEARCH

For Grant N00014-88-K-0341

entitled

CONTINUED DEVELOPMENT AND CHARACTERIZATION OF DOPED LAYERS, CONTACTS AND ASSOCIATED ELECTRONIC DEVICES IN SILICON CARBIDE

For the Period 1 JULY 1989 - 31 DECEMBER 1989

REPORT DOCUMENTATION PAGE

Form Approved
OMB No. 0704-0188

1. AGENCY USE ONLY (Leave blank)	2. REPORT DATE	3. REPORT TYPE AND DATES COVERED
	28 February 1990	Semi-annual/progress 7/1/89-12/31/89

4. TITLE AND SUBTITLE

Continued Development & Characterization of Doped Layers, Contacts & Associated Electronic Devices in Silicon Carbide

5. FUNDING NUMBERS

N00014-88-K-0341

212k003---03/07 DEC 1988 /1212

AB 1791319.W135 000

RA212 0 068342 2B 000000

034450008020 FRC: 212k

6. AUTHOR(S)

Robert F. Davis
John W. Palmour

7. PERFORMING ORGANIZATION NAME(S) AND ADDRESS(ES)

North Carolina State University, Hillsborough Street, Raleigh, NC 27695 and Cree Research Inc.,2810 Meridan Parkway, Suite 176 Durham, NC 27713.

8. PERFORMING ORGANIZATION REPORT NUMBER

9. SPONSORING/MONITORING AGENCY NAME(S) AND ADDRESS(ES)

Office of Naval Research
800 North Quincy Street
Arlington, VA 22217-5000

10. SPONSORING/MONITORING AGENCY REPORT NUMBER

11. SUPPLEMENTARY NOTES

12a. DISTRIBUTION/AVAILABILITY STATEMENT

Approved for Public Release; Distribution Unlimited

12b. DISTRIBUTION CODE

13. ABSTRACT *(Maximum 200 words)*

Electronic devices for microwave applications, the science and technology of ohmic and Schottky contacts and equipment fabrication for ultra-high purity thin films have been the subjects of concern for the application of growth of the 6H SiC polytype in this reporting period. MESFETs having gate lengths of 2, 4, 13 and 24 microns with maximum transconductances in the range of 1.5-22 ms/mm, respectively and with very low subthreshold leakage currents were fabricated. The 2 micron device also had threshold frequency of 510 MHz at 0dB gain; the power gain crossed 0dB at approximately 380 MHz. IMPATT based on Schottky diodes showed permanent breakdown; those based on p-n junctions appear promising. Ohmic and Schottky contacts are important for devices; thus, a program to examine the interface chemistry and associated electrical properties of high purity contacts deposited under controlled conditions, have been initiated. A molecular beam epitaxy system for the deposition of high purity SiC films is also nearing completion.

14. SUBJECT TERMS

Silicon carbide, MESFETs, IMPATTs, Ohmic Contacts, Schottky Contacts, molecular beam epitaxy

15. NUMBER OF PAGES

40

16. PRICE CODE

17. SECURITY CLASSIFICATION OF REPORT	18. SECURITY CLASSIFICATION OF THIS PAGE	19. SECURITY CLASSIFICATION OF ABSTRACT	20. LIMITATION OF ABSTRACT
UNCLAS	UNCLAS	UNCLAS	SAR

GENERAL INSTRUCTIONS FOR COMPLETING SF 298

The Report Documentation Page (RDP) is used in announcing and cataloging reports. It is important that this information be consistent with the rest of the report, particularly the cover and title page. Instructions for filling in each block of the form follow. It is important to ***stay within the lines*** to meet ***optical scanning requirements***.

Block 1. Agency Use Only *(Leave blank)*.

Block 2. Report Date. Full publication date including day, month, and year, if available (e.g. 1 Jan 88). Must cite at least the year.

Block 3. Type of Report and Dates Covered. State whether report is interim, final, etc. If applicable, enter inclusive report dates (e.g. 10 Jun 87 - 30 Jun 88).

Block 4. Title and Subtitle. A title is taken from the part of the report that provides the most meaningful and complete information. When a report is prepared in more than one volume, repeat the primary title, add volume number, and include subtitle for the specific volume. On classified documents enter the title classification in parentheses.

Block 5. Funding Numbers. To include contract and grant numbers; may include program element number(s), project number(s), task number(s), and work unit number(s). Use the following labels:

C -	Contract	**PR** -	Project
G -	Grant	**TA** -	Task
PE -	Program Element	**WU** -	Work Unit Accession No.

Block 6. Author(s). Name(s) of person(s) responsible for writing the report, performing the research, or credited with the content of the report. If editor or compiler, this should follow the name(s).

Block 7. Performing Organization Name(s) and Address(es). Self-explanatory.

Block 8. Performing Organization Report Number. Enter the unique alphanumeric report number(s) assigned by the organization performing the report.

Block 9. Sponsoring/Monitoring Agency Name(s) and Address(es). Self-explanatory.

Block 10. Sponsoring/Monitoring Agency Report Number. *(If known)*

Block 11. Supplementary Notes. Enter information not included elsewhere such as: Prepared in cooperation with...; Trans. of...; To be published in.... When a report is revised, include a statement whether the new report supersedes or supplements the older report.

Block 12a. Distribution/Availability Statement. Denotes public availability or limitations. Cite any availability to the public. Enter additional limitations or special markings in all capitals (e.g. NOFORN, REL, ITAR).

- **DOD** - See DoDD 5230.24, "Distribution Statements on Technical Documents."
- **DOE** - See authorities.
- **NASA** - See Handbook NHB 2200.2.
- **NTIS** - Leave blank.

Block 12b. Distribution Code.

- **DOD** - Leave blank.
- **DOE** - Enter DOE distribution categories from the Standard Distribution for Unclassified Scientific and Technical Reports.
- **NASA** - Leave blank.
- **NTIS** - Leave blank.

Block 13. Abstract. Include a brief *(Maximum 200 words)* factual summary of the most significant information contained in the report.

Block 14. Subject Terms. Keywords or phrases identifying major subjects in the report.

Block 15. Number of Pages. Enter the total number of pages.

Block 16. Price Code. Enter appropriate price code *(NTIS only)*.

Blocks 17. - 19. Security Classifications. Self-explanatory. Enter U.S. Security Classification in accordance with U.S. Security Regulations (i.e., UNCLASSIFIED). If form contains classified information, stamp classification on the top and bottom of the page.

Block 20. Limitation of Abstract. This block must be completed to assign a limitation to the abstract. Enter either UL (unlimited) or SAR (same as report). An entry in this block is necessary if the abstract is to be limited. If blank, the abstract is assumed to be unlimited.

I. INTRODUCTION

Silicon carbide is the only compound species that exists in the solid state in the Si-C system, however it can occur in many polytype structures. The lone cubic polytype crystallizes in the zincblende structure and is denoted as beta-SiC. The approximately 170 known additional hexagonal and rhombohedral polytypes are collectively referred to as alpha-SiC. The most common of these latter polytypes is 6H-SiC where the 6 refers to the number of Si-C bilayers along the closest packed direction and H the hexagonal crystal structure.

Silicon Carbide is considered a superior candidate material for high temperature, high power and high frequency electronic devices due to its high melting point, high thermal conductivity (4.9W/cm°C), wide bandgap (2.86 eV for 6H-SiC) and high breakdown field (2 - 3 x 10^6 V/cm). Additional reasons for the renewed interest in silicon carbide are the significant advances in the growth of single crystal boules of the 6-H polytype, the deposition of monocrystalline thin films of both the beta and the 6-H polytypes of this material by chemical vapor deposition (CVD), the ability to dope this material with n- and p-type dopants during growth or via ion implantation, the existence of a native oxide, the ability to reactive ion etch the material with NF_3, and the ability to use device fabrication procedures similar to those of Si technology. As a result, devices from this material have now become a reality.

In this reporting period, the fabrication of electronic devices for microwave applications, the science and technology of ohmic and Schottky contacts and equipment fabrication for ultra-high purity thin films have been the subjects of research. The devices include MESFETs having various gate lengths and IMPATTs from Schottky and p-n junction - based structures. A program to examine the interface chemistry of selected ohmic and Schottky contacts on alpha-SiC and to correlate this knowledge with electrical properties has been initiated. Finally, a molecular beam epitaxy system for the deposition of high purity SiC films has also been designed and fabrication is nearing completion. The following sections detail the procedures and results of this work to date and chart a course of future research.

II. DEVICES FOR MICROWAVE APPLICATIONS

A. Introduction

The SiC polytype that currently shows the most promise for high power microwave performance is 6H-SiC. The reason for this choice lies in the high quality and availability of this material more than in its basic electrical properties. For instance, an IMPATT diode relies on operation of a diode in avalanche; while very good avalanche characteristics can now be attained with pn junction diodes in 6H-SiC, no avalanche characteristics have been reported for β-SiC diodes. Likewise, no stable MESFET characteristics have been reported for β-SiC for drain voltages higher than 10 V, while 6H-SiC MESFETs reported herein are able to withstand drain voltages as high as 100 V. The ability to operate at these higher fields is key to the success of SiC at high frequencies. Because of the excellent crystal quality of 6H-SiC currently being produced by Cree Research, devices fabricated from this material can operate reliably in these high fields.

The importance of high field operation for SiC microwave performance is two-fold. The first is to obtain the high power levels that are desired at high frequency without having to make an inordinately large device. The second reason is to take advantage of the high saturated electron drift velocity (v_{sat}) of SiC (2.5×10^7 cm/sec) observed at fields above about 1.5×10^5 V/cm, as shown in Fig. 1. For a MESFET operated with a source-to-drain field greater than this value, the transfer characteristics will be dominated more by v_{sat} than mobility, which is quite low in SiC when compared with Si or GaAs. For an IMPATT diode, the high field capability of SiC obviously allows much more power per unit area to be delivered because it is avalanching at much higher voltages than equivalent Si or GaAs diodes, and the high v_{sat} allows higher frequency operation.

As discussed previously, the two most promising devices for microwave performance of SiC are MESFETs and IMPATT diodes. If a high voltage SiC MESFET is to be fabricated, the first requirement is to have a high voltage Schottky contact; the second requirement is that this Schottky contact must operate reliably at elevated temperatures because of the high power levels anticipated for these devices. While Au Schottky contacts have been shown to be quite good for both β-SiC[1,2] and 6H-SiC at room temperature, they have also been shown to degrade rapidly with elevated temperatures[2], in the range of 300°C. Therefore, a more stable Schottky contact is required for a high power microwave device. Viability of this contact in a high voltage MESFET must then be proven, and finally a high power microwave device can be designed and fabricated.

Likewise, if a high frequency IMPATT diode is to be fabricated in SiC, then reliable avalanche characteristics must first be proven. Once the best configuration for avalanche operation is

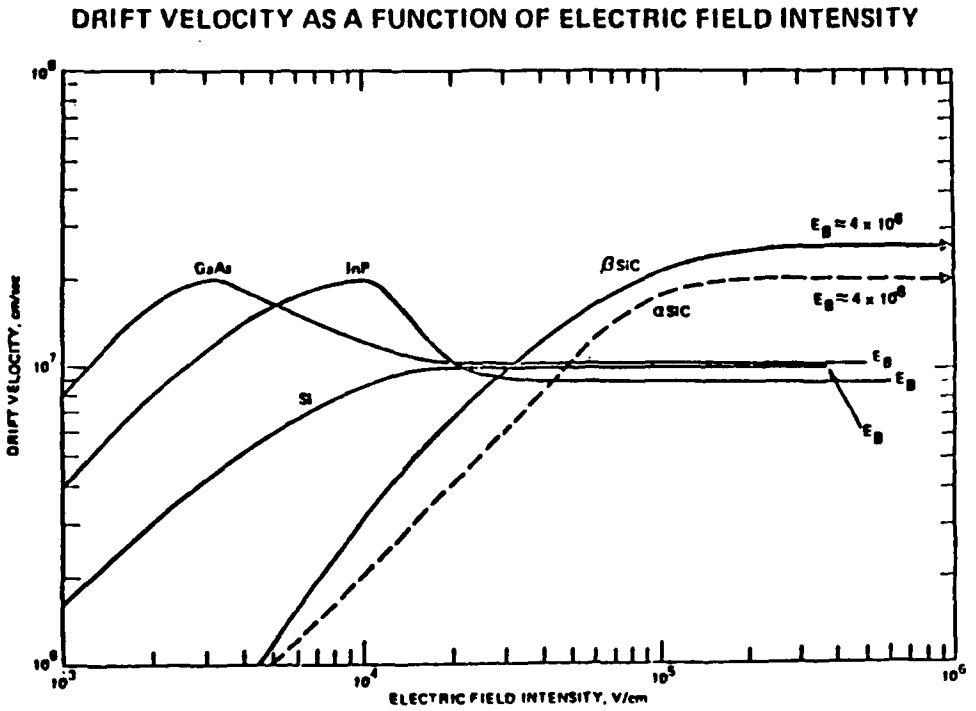

Figure 1: Electron velocity vs. electric field for several semiconductors.

defined, then an IMPATT diode can be fabricated. These first steps of development for both high frequency MESFETs and IMPATT diodes have been achieved and will be discussed in this report.

B. Experimental Procedure

1. Introduction

The substrates used for this study were sliced from 6H-SiC crystals grown for this project. The crystals were lightly nitrogen doped n-type. The crystals were then sliced, lapped and polished into wafers suitable for epitaxial growth.

Thin films (2 - 3 μm thick) of monocrystalline 6H-SiC (0001), both p- and n-type, were epitaxially grown on these n-type 6H-SiC (0001) wafers. The samples used for Schottky contact research were n-type epilayers on n-type substrates. The samples used for fabricating MESFETS were n-type epilayers on p-type epilayers, grown on n-type substrates. Each wafer was chemically cleaned prior to device processing.

2. MESFETs

Schottky contact samples were first characterized in order to determine the effectiveness of Pt based contacts on 6H-SiC (Pt has been reported to be a very stable Schottky for β-SiC[3]), and to see the effect of carrier concentration on these contacts. The contacts were fabricated by patterning a layer of photoresist such as to leave "doughnuts" of photoresist on n-type epilayers. The Schottky metal, Pt, was then deposited over the entire top surface. The samples were then placed in acetone which dissolved the underlying photoresist and allowed the overlying metal to "lift off" of the doughnuts. This resulted in a series of 100 μm diameter Pt dots, which act as the Schottky contacts, separated from a field of the same metal, which acts as the ohmic contact by virtue of its much larger area.

An interdigitated structure, shown in Figure 2 was used for the initial MESFET design, in order to confirm the high voltage, high power capabilities using the Pt Schottky contact on 6H-SiC. The source consisted of three "fingers" of ohmic contacts on the left, and the smaller area drain consisted of the two fingers of ohmic contacts on the right. Weaving in between these two contacts was the gate or Schottky contact. Isolation trenches were etched in the n-type top conducting layer in order to prevent leakage current around the gate contact between the source and drain. While the gate width was 1 mm for all devices, the gate length and source-to-drain distance was varied in order to determine their effect on transconductance and to be able to extrapolate what the values would be for microwave devices with much smaller dimensions. The different gate

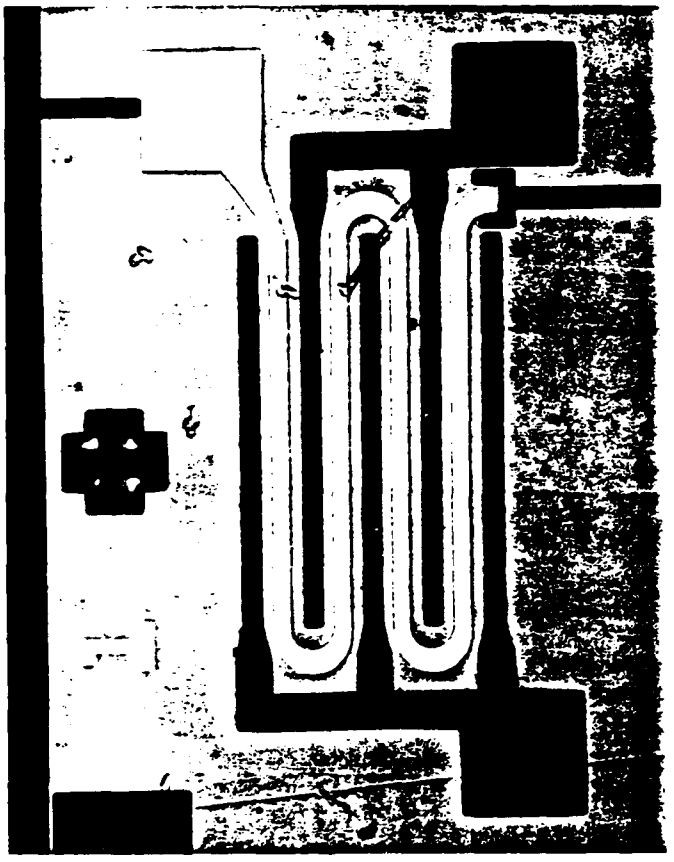

Figure 2: Interdigitated structure of a SiC MESFET. The source contact pad is at the lower left, the drain contact at the lower right, and the gate contact pad is at the upper right. This device has a gate length and width of 10 mm and 1000 mm, respectively.

lengths were 10 um, 13 μm, 18 μm and 24 μm, with the source-to-drain distance being 30 μm, 33 μm, 38 μm and 44 μm, respectively.

In cross-section, the device consisted of a 2 μm thick p-type expitaxial layer of 6H-SiC having a carrier concentration in the range of 1×10^{17} cm^{-3} grown on a 6H-SiC substrate. This p-type layer acted as the buried layer to confine the current to a thin n-type active region which was subsequently grown. This top n-type epitaxial layer can have a carrier concentration in the range of 3×10^{16} cm^{-3} to 3×10^{17} cm^3 and a thickness of 0.2 to 1.0 μm depending on the desired performance of the device.

Using conventional photolithography techniques, a sputtered aluminum film was patterned onto the SiC surface, which acted as a mask with which to open windows for the reactive ion etching of the isolation trenches. The trenches were etched deep enough to penetrate through the top n-type layer into the buried p-type layer. The Al was then stripped, and the sample was oxidized to grow a thin passivating layer of SiO_2. Windows for the source and drain contacts were then opened in the SiO_2 and the ohmic contacts were deposited and patterned using the "lift-off" technique. After these ohmic contacts were annealed, the gate Schottky contact was deposited in similar fashion. Unless heat treatment of the gate contact was desired, the device was then ready for measurement.

The initial design of a high power-high frequency SiC MESFET is shown in Fig. 3. The device has large area source and drain contacts in order to reduce the contact resistance, and the source-to-drain distances are all much smaller, ranging from 7 μm down to 2 μm. The gate contact lengths range from 4 μm down to 0.8 μm. The gate width is 1 mm for all of the devices. The entire device is isolated on a mesa as opposed to fabricating isolation trenches. All other device fabrication procedures are similar to those described for the previous MESFET design. For simplicity, the initial devices were fabricated with the gate contact pad patterned at the same time as the gate pattern, simply being a large area Pt pad on the the SiC surface. Therefore, after the gate was patterned the devices were finished. However, this design resulted in a large gate capacitance (about 80 pF) that could degrade the high frequency characteristics of the device.

In order to reduce gate capacitance, subsequent devices were fabricated by placing a gate contact pad, with reduced area on a layer of silicon nitride. This was achieved by depositing about 300 nm of silicon nitride over the entire surface after the oxidation step. Windows for the the source and drain contacts were then opened by reactive ion etching the nitride, and then etching the SiO_2 and patterning the ohmic contacts as before. After the contacts were annealed, the gate was patterned as discussed earlier (with the addition of the RIE step for the nitride), but the gate

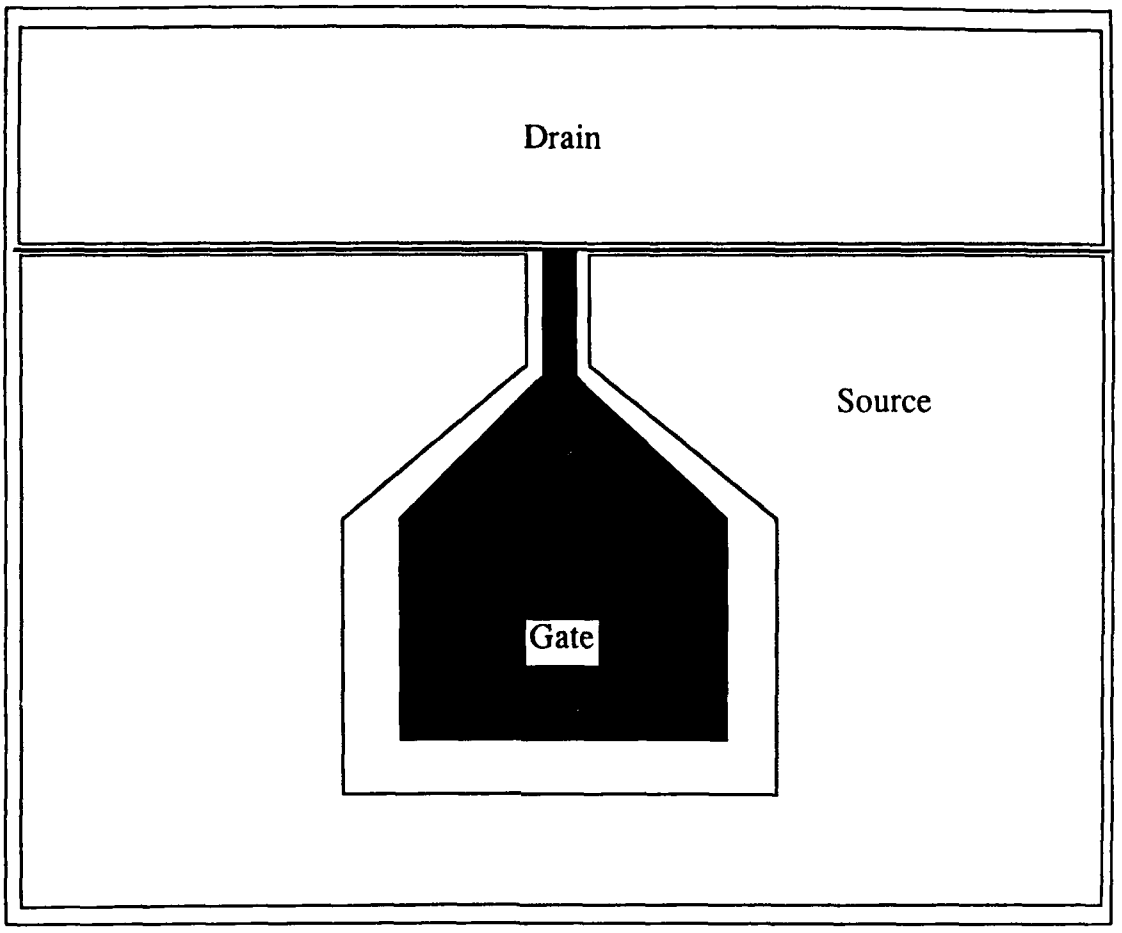

Figure 3: Initial design of high power, high frequency SiC MESFET. Gate lengths vary from 4 mm to 0.8 mm, and source-to-drain distances vary from 7 mm to 2 mm. The gate width is 1 mm.

patterned consisted of only the gate "stripe" with a small 20 mm x 5 mm tab coming off of it, making the actual area of the Schottky contact very small. Contact was then made to the gate by patterning a metal pad on top of the nitride with a strip that drops over the nitride step and overlaps the gate tab. This step reduced the gate capacitance to about 4-6 pF.

3. IMPATT Diodes

Guard ring Schottky diode samples were fabricated for verification of avalanche breakdown induced by Schottky contacts. The guard ring structure, shown in Fig. 4, utilized an Al^+ ion implanted ring of p-type SiC lying under the periphery of the Schottky contact, with the intent of preventing the edge corona typically associated with Schottky breakdown. The n-type epilayer (3.5×10^{16} cm^{-3}) was grown on an n^+ substrate, and an ohmic contact (Ni) was deposited on the backside of this substrate, imitating the vertical structure of an IMPATT diode. The platinum Schottky contacts were then patterned on the epilayer using the "lift-off" process, leaving 0.66 mm x 0.66 mm squares to define the diode dimensions.

The initial modeling for IMPATT diodes was for operation at 60 GHz using a flat profile for the drift layer, and showed that this epilayer must have $n = 4 \times 10^{16}$ cm^{-3} and a thickness of 2 μm. This thickness and carrier concentration are dictated by that desired frequency. Unfortunately, the carrier concentration in turn dictates that the avalanche will occur at voltages in the range of 350-400 V for SiC. This is a demanding voltage from the aspect of junction quality and passivation. While these voltages have certainly been achieved for SiC pn junction diodes, it requires special structures and passivation techniques that may not readily transfer into a desirable IMPATT fabrication scheme. Therefore, more modeling was performed so that a "high-low" structure could be used, in which the avalanche takes place at a relatively low voltage in a more heavily doped layer, and the drift takes place in a more lightly doped layer. The modeling showed the most desirable doping profile for a high-low structure is a 0.2 μm thick "high" layer with $n = 4.5 \times 10^{17}$, and a 1.2 μm thick "low" layer with $n = 3 \times 10^{16}$ cm^{-3}. Both the "flat" profile and the "high-low" structure are being fabricated at present. Regardless of the breakdown structure, the same set of masks are used. Seven different diameter dots, varying from 38.1 μm to 381 μm, were designed in order to find the device area that yielded the best impedance matching.

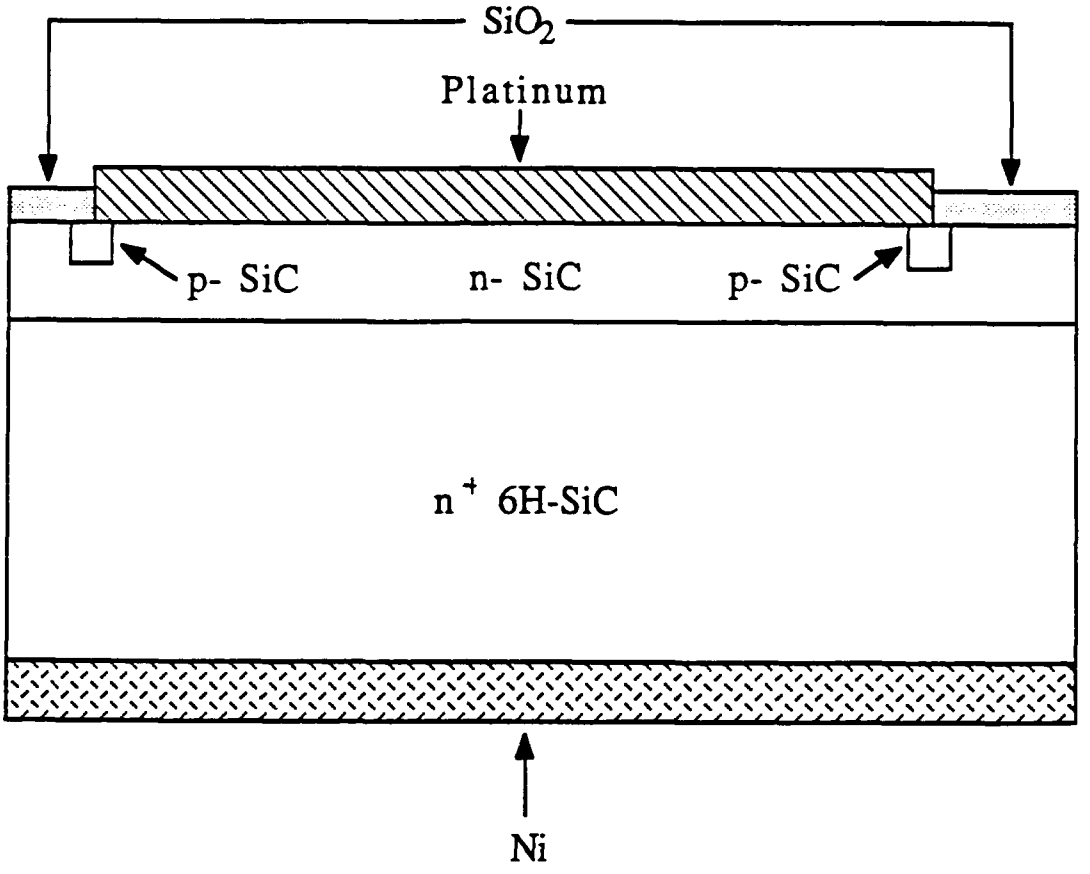

Figure 4: Cross-sectional view of guard ring structure used for a vertical Schottky diode.

C. RESULTS AND DISCUSSION

1. Schottky Contact Testing

Schottky contact research was first conducted because this is the fundamental building block of a MESFET. Both platinum and gold contacts were deposited and characterized. The gold acted as a "control" contact for the platinum experiments, because gold Schottkys on SiC have been previously characterized. While providing very good rectifying characteristics at room temperature, the gold contacts permanently degraded when heated above 300°C, as was noted in the previous studies. Conversely, the platinum Schottky contacts demonstrated very good rectifying characteristics in both the as-deposited condition and after annealing at a variety of temperatures.

Different n-type concentrations were investigated for use as the conducting channel of a MESFET, with the emphasis on the effect carrier concentration had on the leakage current and the breakdown voltage of the Schottky diode. The Pt Schottkys on n-type SiC with $n = 4x10^{16}$ cm^{-3} generally experienced breakdown at reverse bias of -85 V to -92 V. This corresponds to a maximum field strength greater than 6×10^5 V/cm, which is higher than Si or GaAs can even theoretically achieve. For an annealed Pt Schottky on a sample with $n = 6 \times 10^{16}$ cm^{-3}, breakdown occurred at -70 V reverse bias and the leakage current remained quite low (<1 μA) at voltages below this, as shown in Figure 5. Samples were also measured on films with $n = 1 \times 10^{17}$ cm^{-3} and $n = 3.3 \times 10^{17}$ cm^{-3}, the latter of which is shown in Figure 6. This shows that for reverse biases less than -30 V, films doped as high as 3.3×10^{17} cm^{-3} could be used for MESFETs, which should allow very high transconductances (very low resistive losses). Even with this high doping level the Schottky did not truly breakdown until a reverse bias of -46 V was reached. Even more encouraging was the fact that these curves remained almost identical when the devices were heated to 400°C, showing excellent temperature stability.

2. MESFET Testing

Many MESFET samples were fabricated, all of which worked with varying degrees of success. The best results are discussed below.

As a result of the Schottky contact research discussed previously, MESFETs were subsequently fabricated. An I-V curve of one of these SiC MESFETs at room temperature is shown in Figure 7(a). This device had a gate length of 13 μm, a gate width of 1 mm, and a source to drain distance of 33 μm. The device shows good current saturation to $V_D = 40$ V, although

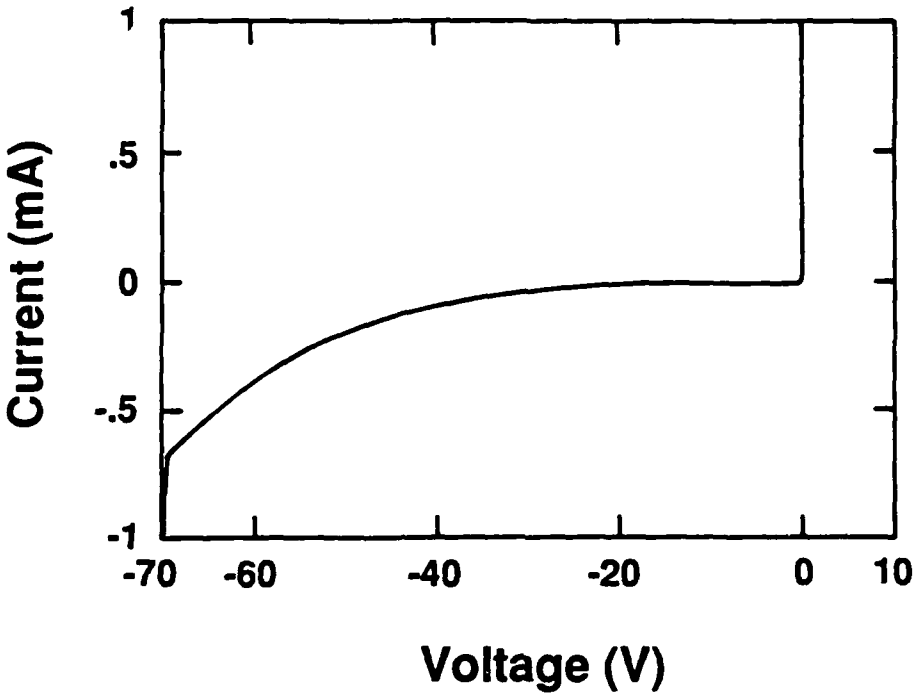

Figure 5: Current-voltage characteristics of an annealed Pt Schottky diode on n-type 6H-SiC with a carrier concentration of $n = 6x10^{16}$ cm^{-3}.

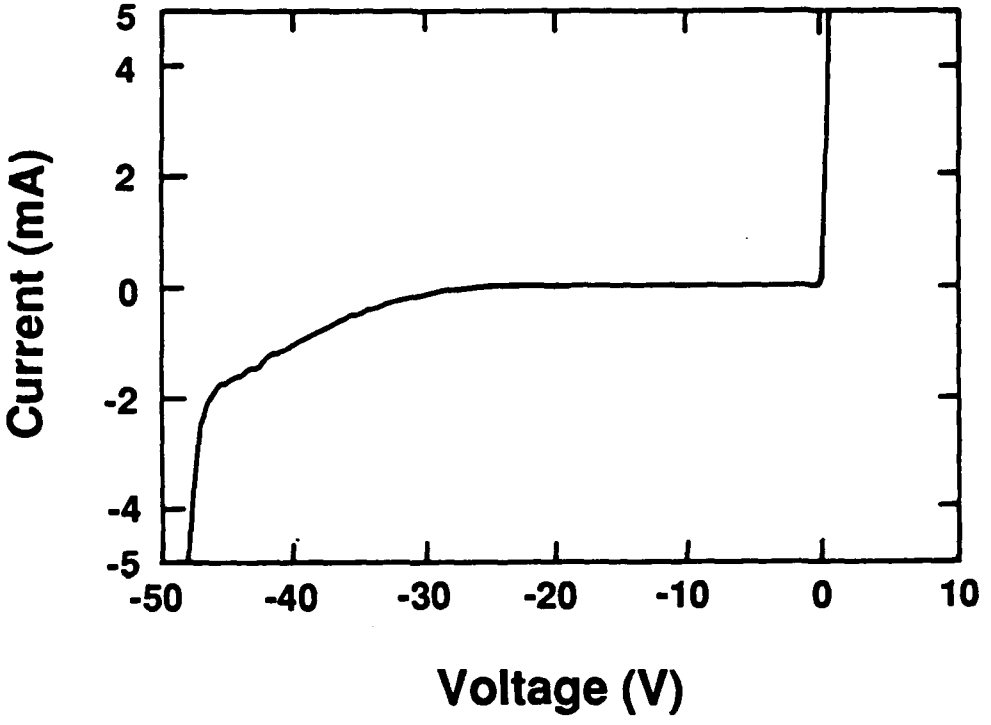

Figure 6: Current-voltage characteristics of an annealed Pt Schottky diode on n-type 6H-SiC with a carrier concentration of $n = 3.3 \times 10^{17}$ cm^{-3}.

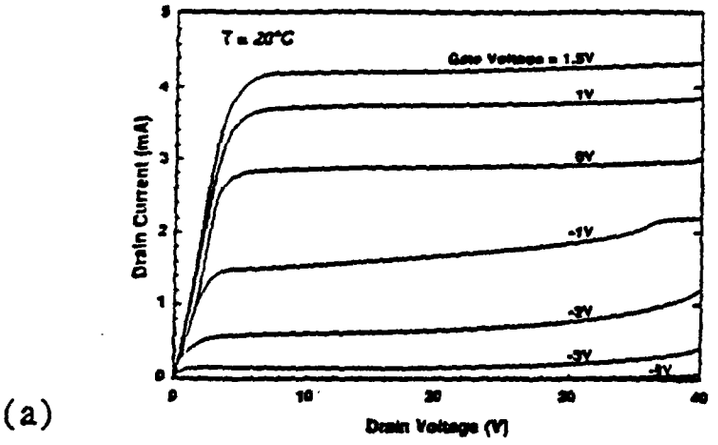

(a)

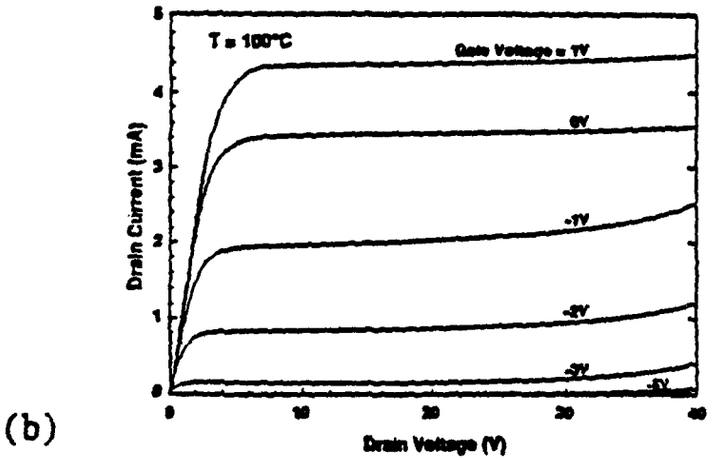

(b)

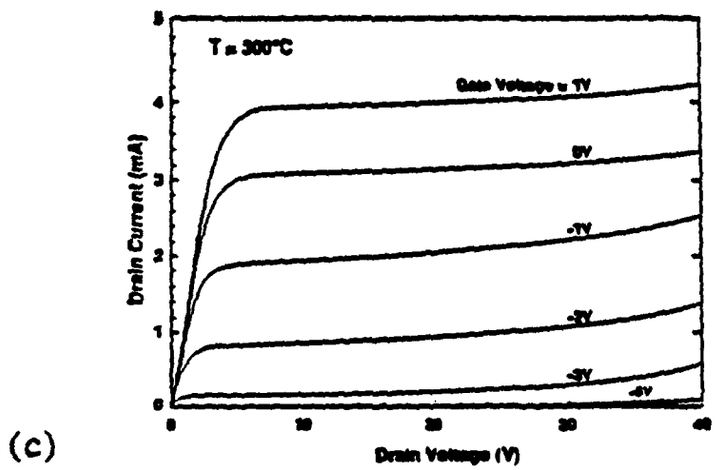

(c)

Figure 7: Drain current-voltage characteristics, after an anneal, of a SiC MESFET at (a) 20°C, (b) 100°C, and (c) 300°C.

there is some non-uniformity at the intermediate gate voltages. The maximum transconductance was 1.5 mS/mm and the threshold voltage is -4.4 V. The subthreshold leakage is quite low, having a value of 44 mA at V_D = 40 V and V_G = -6 V. The MESFET's I-V characteristics actually improved when heated to 100°C, as shown in Figure 7(b). The maximum transconductance increased to 1.65 mS/mm, and the current saturation was quite good to V_D = 30 V, with some leakage still present at higher drain voltages. The subthreshold leakage current was 52 μA at V_D = 40 V and V_G = -6 V. When heated at 200°C, the I-V characteristics were virtually identical to those shown at 100°C. The I-V characteristics at 300°C are shown in Figure 7(c). The subthreshold leakage increased to 96 μA at V_D = 40 V and V_G = -6 V, and the maximum transconductance decreased to 1.26 mS/mm, but overall these were promising characteristics. While these particular devices also operated at 400°C, they were unfortunately ruined by holding at this temperature for too long in air. However, it is assumed that if the device was hermetically sealed in a package containing an inert atmosphere, that the devices would have operated to much higher temperatures, indicating that high power MESFETs will withstand a large amount of self-heating.

Improved control over doping and crystal quality led to the fabrication of MESFETs with improved high voltage capability, as shown in Fig. 8. This device had a source-to-drain distance of 44 μm and a gate length of 24 μm. Drain voltages of 100 V were achieved without breakdown or significant leakage. The current levels were also quite high compared to those shown in Fig. 7, with power capability at a drain voltage of 100 V being in excess of 4 W per mm of gate width. The maximum transconductance was also higher, at 4.3 mS/mm. The subthreshold leakage current at V_d = 100 V and V_g = -18 V was 325 μA. Since high field operation is desired for a SiC high frequency MESFET, these results were very promising. The remaining task is to translate this high field capability of the Schottky gate into a much smaller dimension gate length and a much smaller source-to-drain distance.

Devices with these smaller dimensions have been fabricated using the design illustrated in Fig. 3. The n-type channels had a doping level of n = 0.8-3 x 10^{17} cm^{-3} and a thickness of about 200-400 nm, with buried p-layers (p = 1-4 x 10^{16} cm^{-3}) underneath. A typical I-V curve of one of these MESFETs is shown in Fig. 9. This particular device had a source-drain distance of 4 μm and a gate length of 2 μm. The curve shows that a drain voltage of 30 V was obtained with a gate voltage of -6 V. The maximum transconductance of this device was 6.4 mS/mm and very stable current saturation was observed to V_{DS} = 30 V. This device was measured on at high frequency using an HP 8510 automatic network analyzer with a Cascade Microprober for standard S-parameter measurements. The plot in Fig. 10 shows that this device has a threshold frequency

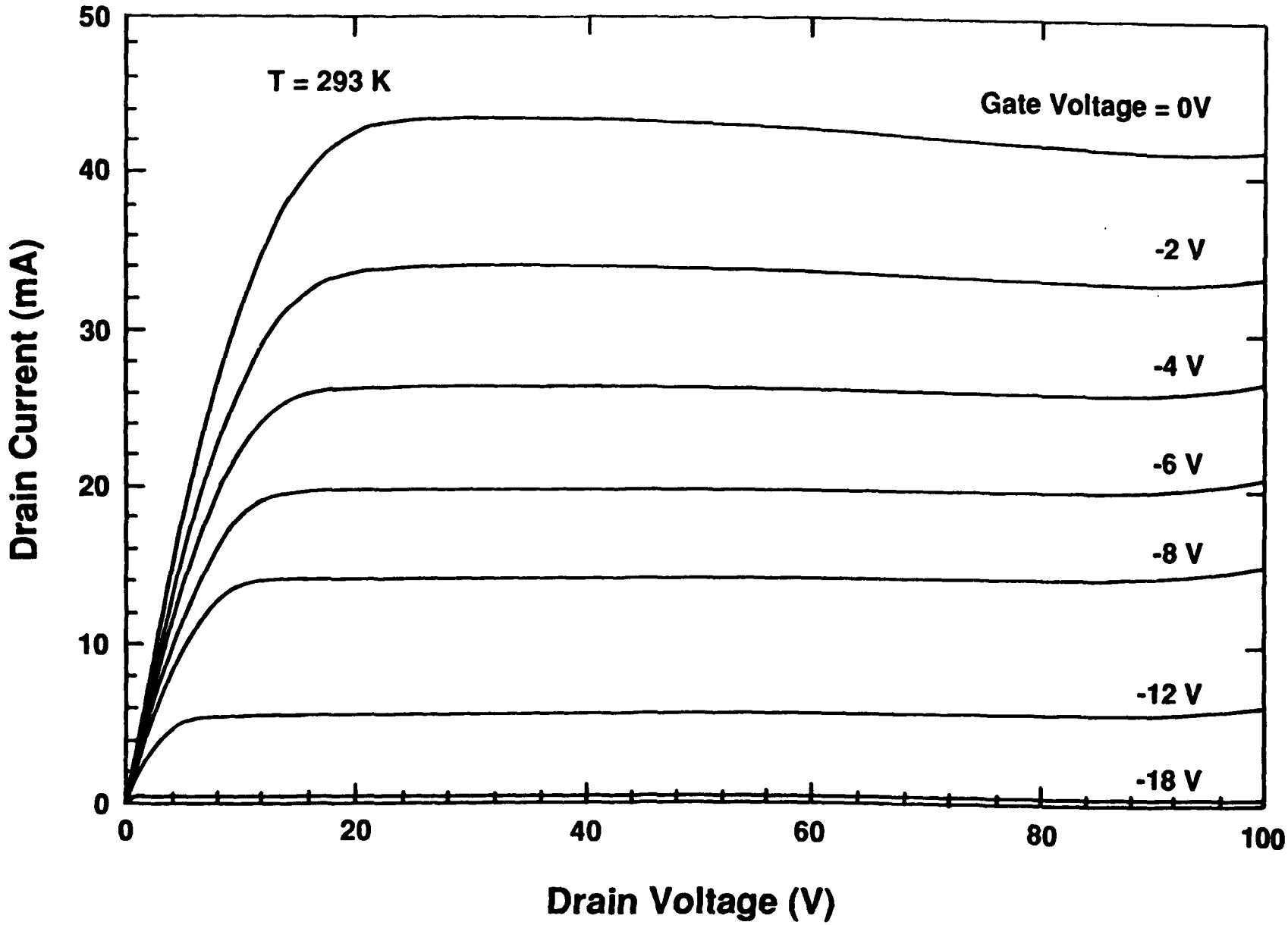

Figure 8: Drain current-voltage characteristics of a SiC MESFET demonstarting V_d = 100 V capability. Gate length and width are 24 mm and 1mm, respectively.

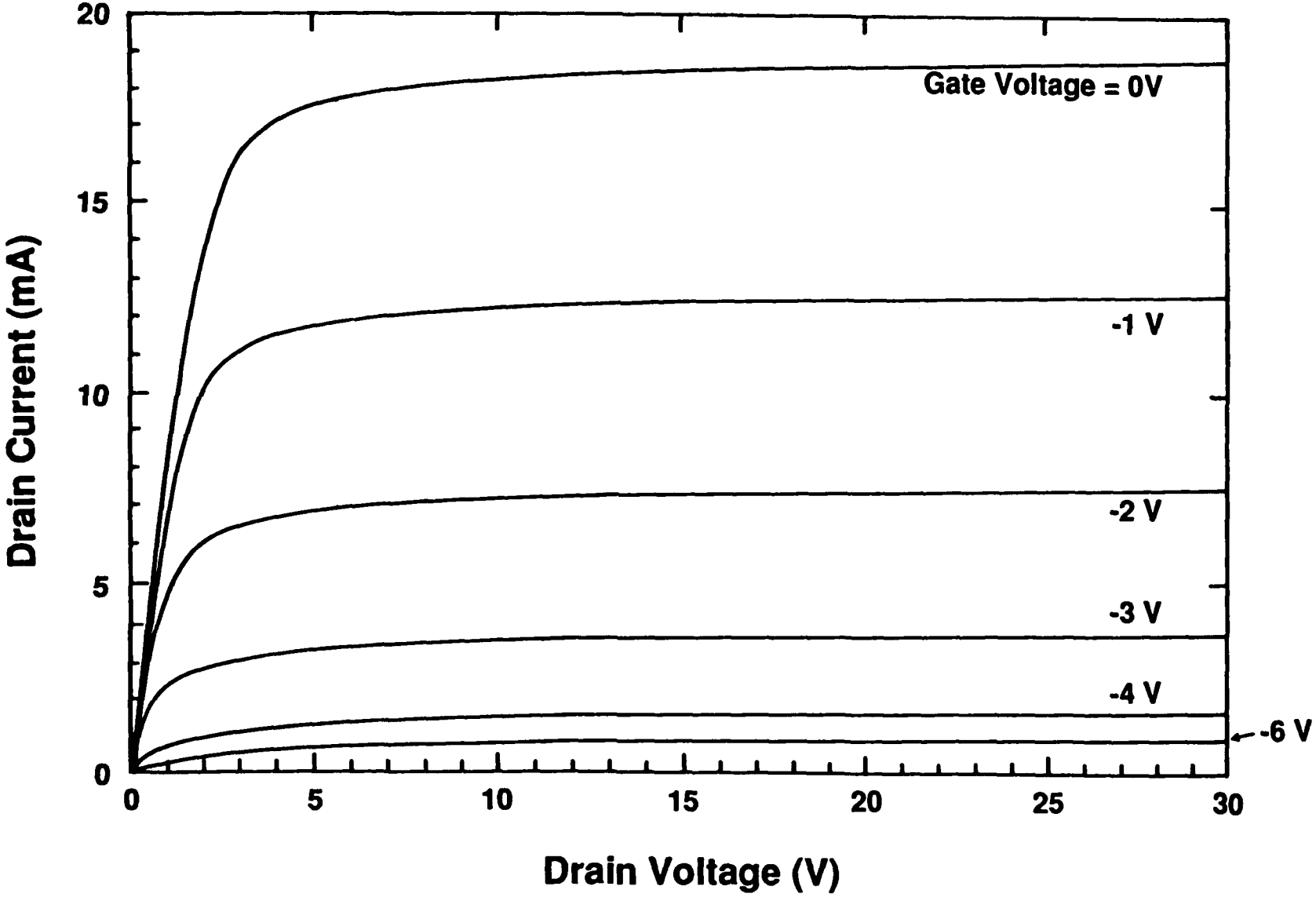

Figure 9: Drain current-voltage characteristics of a SiC MESFET using high power high frequency mask shown in Fig. 3. Gate length and width are 2 mm and 1 mm, respectively. Source-to drain distance is 4 mm. The maximum transconductance is 6.4 mS/mm.

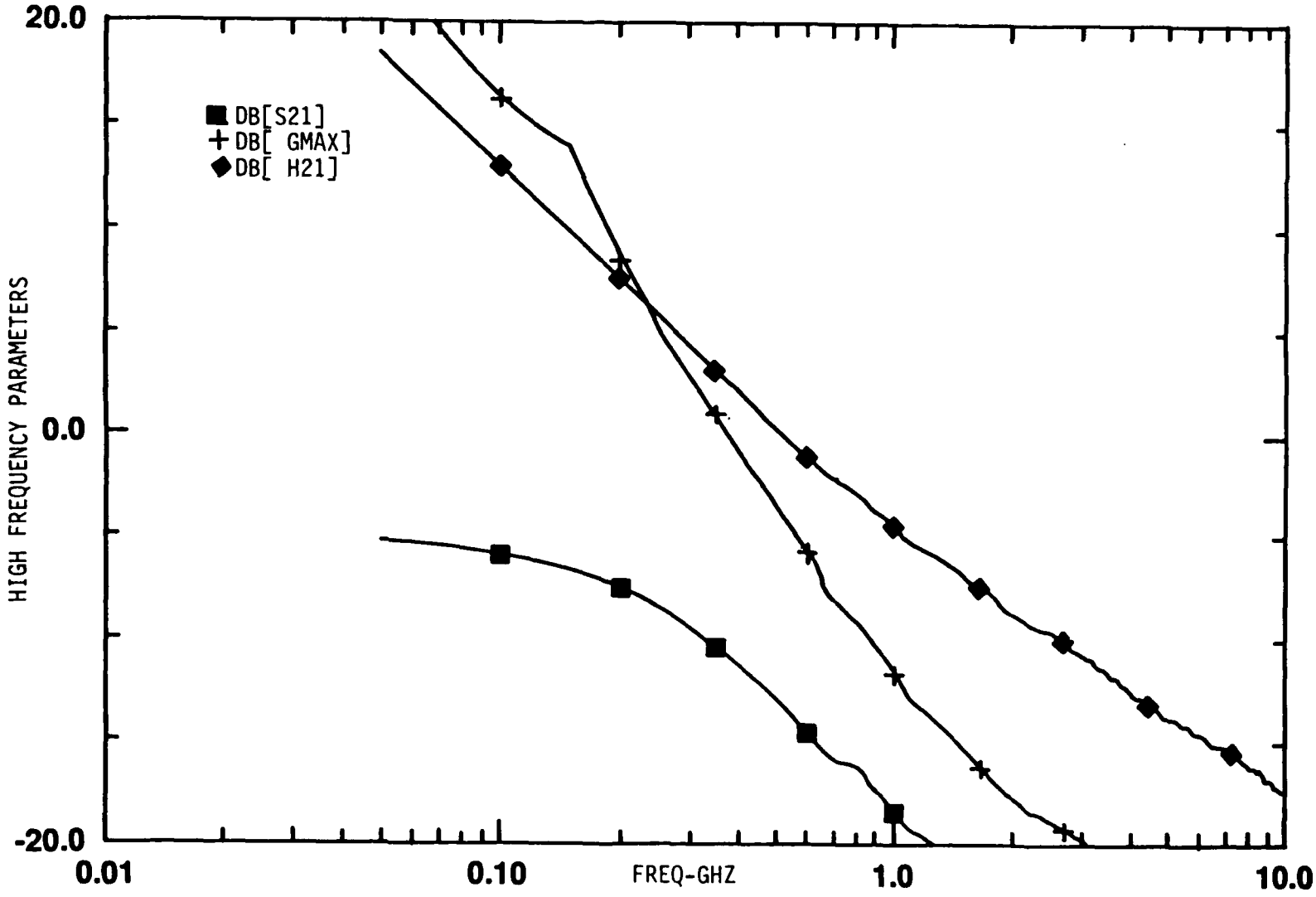

Figure 10: High frequency parameters, S21, G_{max}, and H21, as a function of frequency for the 2 mm gate length device shown in Fig. 9. Measurement conditions were V_D = 30 V, I_D = 14.2 mA, V_G = -1.0 V, and I_G = 1 mA.

(F_t) of 510 MHz, designated where the H21 parameter crosses 0 dB gain. The power gain (G_{max}) crosses 0 dB at about 380 MHz, indicating that F_{max} is at least 380 MHz.

A gain vs. frequency plot for a shorter gate length device is shown in Fig. 11. This device had a gate length of 1.7 μm and had a correspondingly higher gain. The F_t of this device was 800 MHz and the F_{max} was at least 450 MHz. At 250 MHz the device had a current gain of 10 dB. While the high frequency gain always increased with decreasing gate length, as it should, the DC transconductance seemed to be virtually independent of gate length. For instance, the highest transconductance observed to date was 22 mS/mm for a 4 μm gate length device. Figure 12 shows a MESFET with a 2 μm gate length that had a relatively high transconductance of 12.3 mS/mm but still had a relatively short gate length. Although this device had a high on-current (>200 mA), it could not be cutoff because the channel was too thick. This device had the best high frequency gain of the devices measured, as shown in Fig. 13. It had an F_t of 900 MHz and a F_{max} greater than 450 MHz.

The observed DC transconductances were quite low when compared to the long gate length device shown in Fig. 8, considering the much smaller gate lengths and source-drain distances used in the high frequency design. This indicates that the limiting parasitic resistance is not related to mobility between the source and drain, but rather to contact resistance at the source and drain. It is apparent that the source and drain resistance are so dominant that the effect of reducing the gate length and source-drain spacing on the DC transconductance is negligible. The high frequency measurements show the effect of gate length because transit-time still plays a role, however, it is proposed that the overall high frequency gain of all of the devices was severely limited by the parasitic source and drain resistances. As such, the next iteration of 6H-SiC MESFETs will be fabricated with n^+ source and drain wells, as is common practice even for GaAs MESFETs. This will not only greatly reduce the resistivity of the material itself, but will also greatly reduce the contact resistance of the ohmic contacts. Thus, markedly increased frequency capability should result from using n^+ source and drain wells.

3. MESFET Modeling

The positive benefits of n^+ source and drain wells have been confirmed by modeling of similar 6H-SiC MESFETs at high frequency. The RF performance potential of 6H-SiC MESFETs at 0.5, 3, and 10 GHz was investigated. Making conservative assumptions for mobility and contact resistance values, 240 cm^2/V-sec and 1 x 10^{-4} W-cm^2 respectively, and assuming n^+ source and drain wells, maximum power was calculated for each of these frequencies. The assumed dimensions of the device were a 1 μm gate length, a 1 μm source-gate distance, and a 2

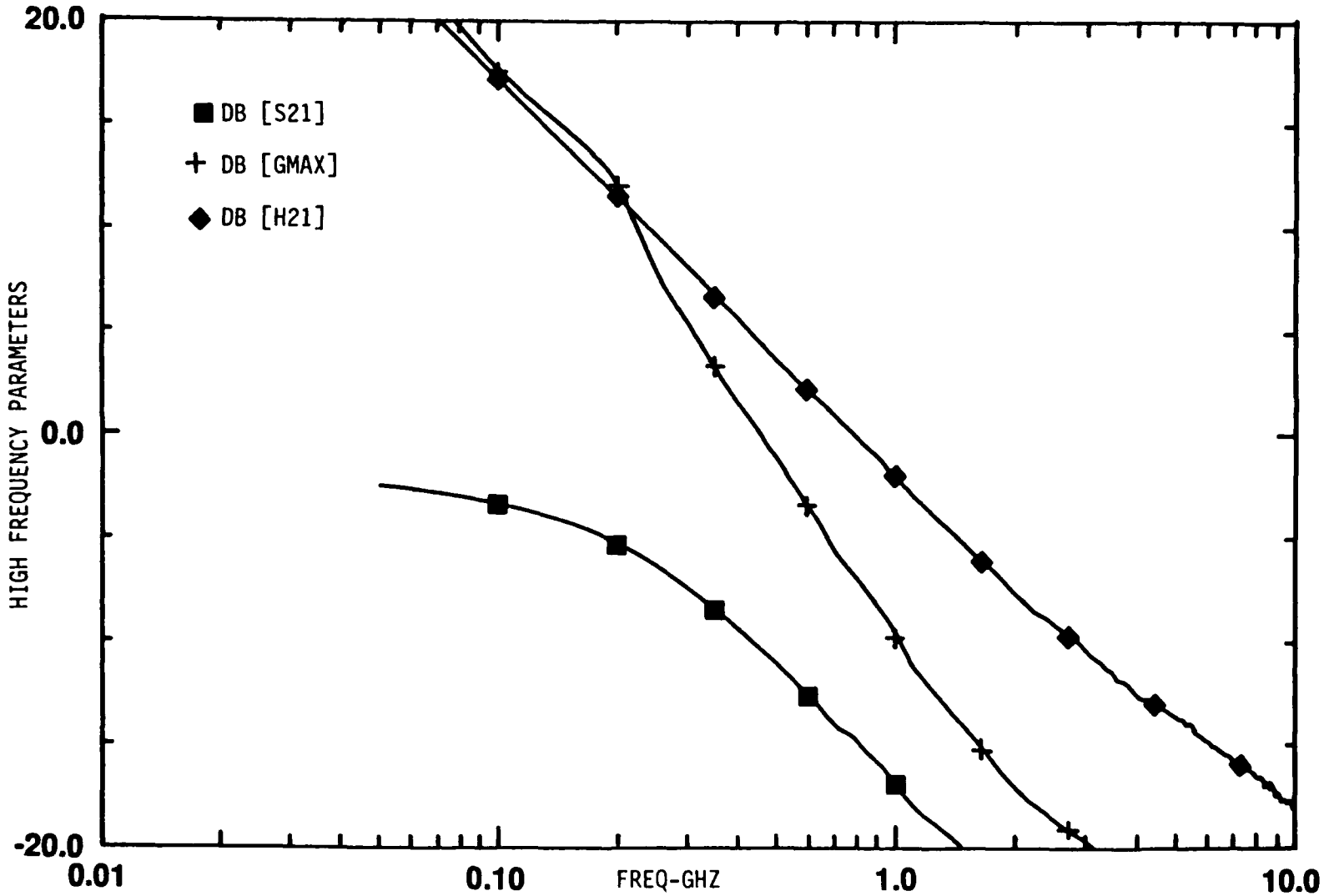

Figure 11: High frequency parameters, S21, G_{max}, and H21, as a function of frequency for a 1.7 mm gate length device. Measurement conditions were V_D = 30 V, I_D = 68.4 mA, V_G = -1.0 V, and I_G = 1.7 mA.

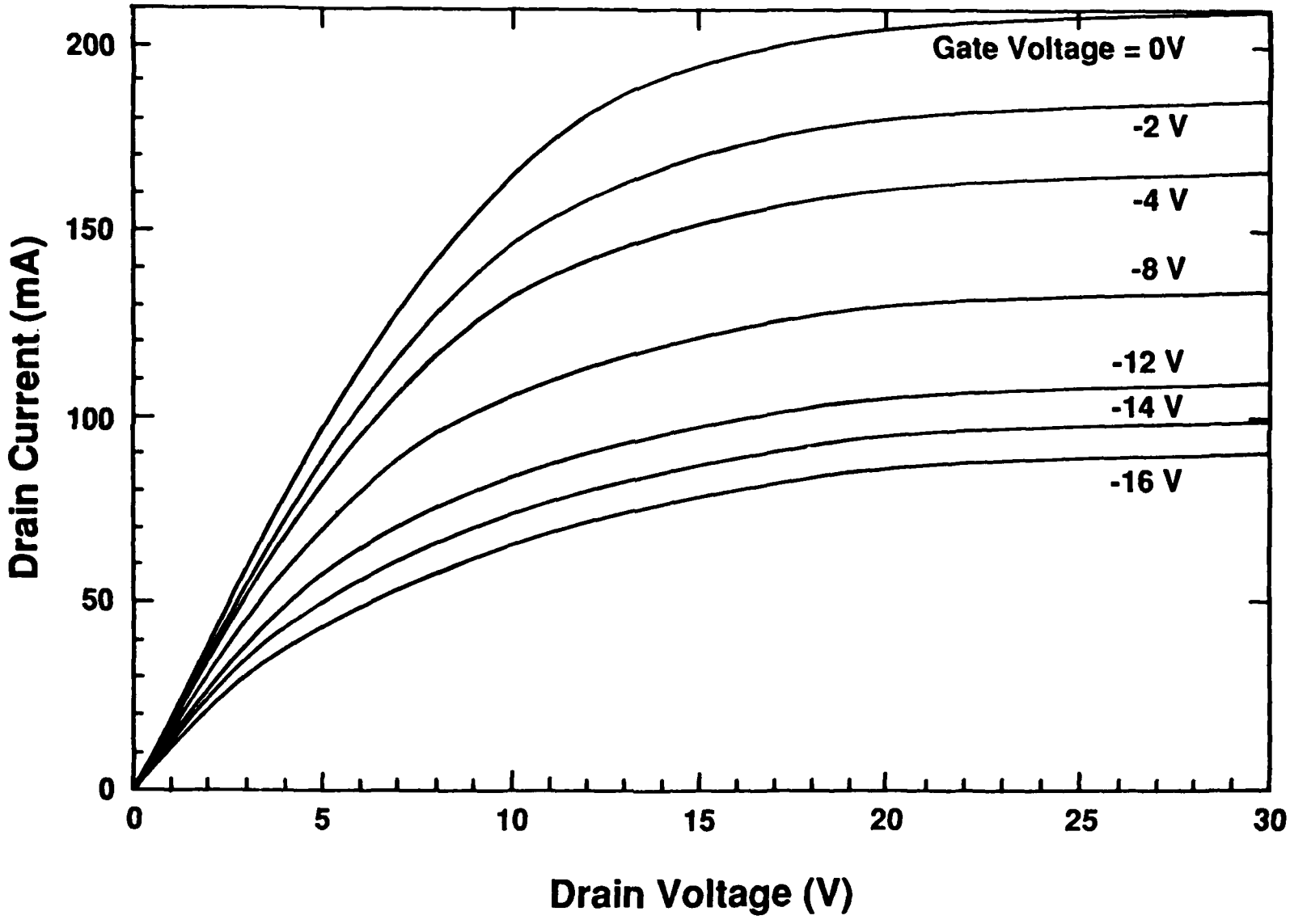

Figure 12: Drain current-voltage characteristics of a SiC MESFET. Gate length and width are 2 mm and 1 mm, respectively. Source-to drain distance is 4 mm. The maximum transconductance is 12.3 mS/mm.

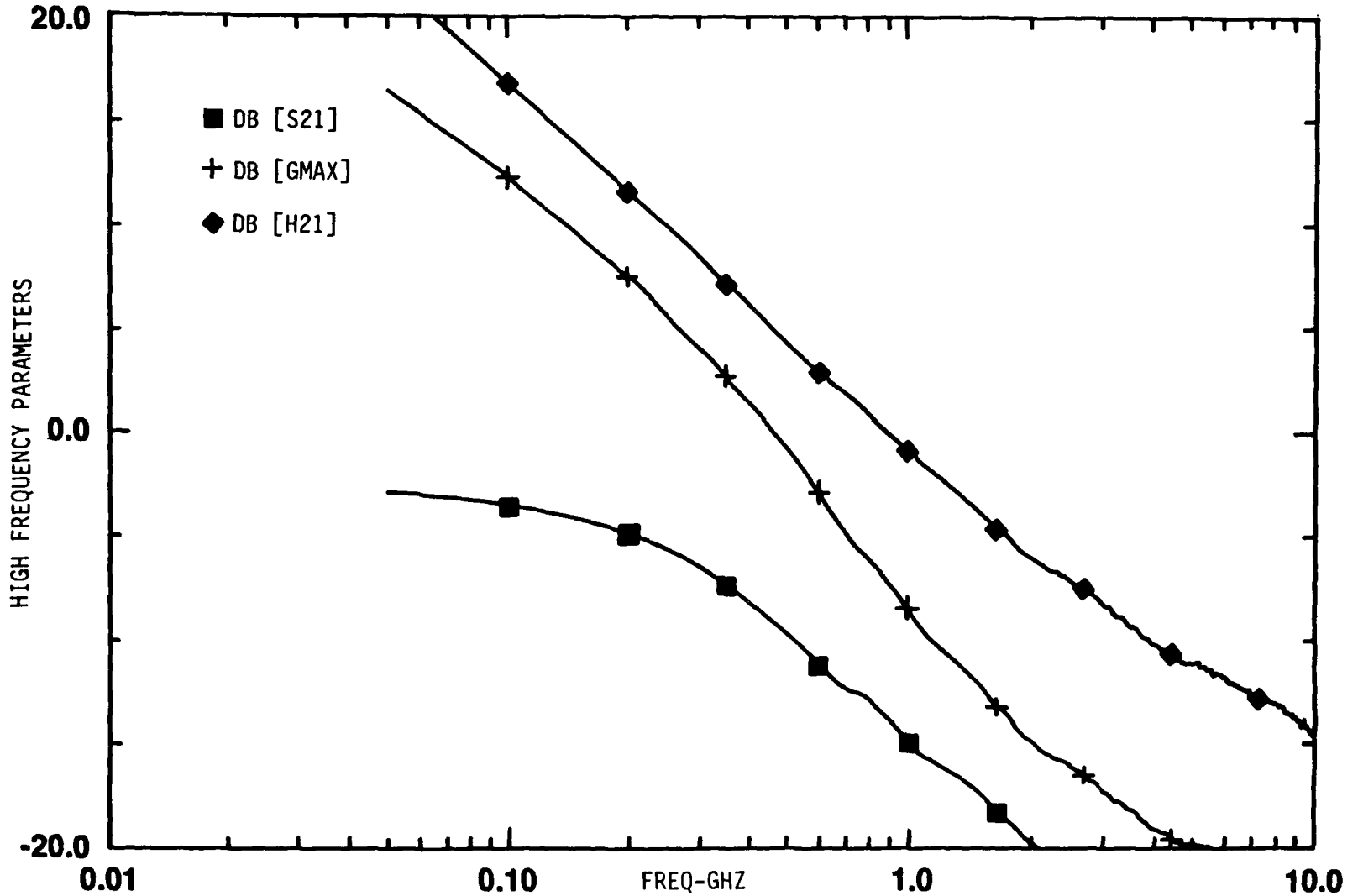

Figure 13: High frequency parameters, S21, G_{max}, and H21, as a function of frequency for the 2 mm gate length device shown in Fig. 12. Measurement conditions were V_D = 30 V, I_D = 189 mA, V_G = -1.0 V, and I_G = 1 mA.

μm gate-drain distance. The 6H-SiC devices produced about 630 W, 158 W and 45 W at those three frequencies, respectively. This corresponds to a normalized RF output power of about 2.5 W/mm of gate length. This value compares quite favorably with the 0.5-0.6 W/mm obtained with GaAs power FETs. Power-added efficiency and gain were also quite good and are shown, along with output power, as a function of frequency in Fig. 14. All devices were biased for class A operation and CW conditions were assumed. Increased output power could be obtained from class B or C operation and/or pulse bias conditions; however, these modes of operation were beyond the scope of this investigation. Due to the excellent thermal conductivity of SiC, thermal modeling of the MESFETs showed that they are not thermally limited and should, in fact, be operable at elevated temperatures.

4. IMPATT Diodes

As a first step to determining if Schottky contacts could be used for IMPATT diode structures, reliable avalanche conditions have to be demonstrated for a Schottky diode. Based on previous work performed at Cree Research, no non-damaging avalanche characteristics had been demonstrated for simple Schottky diode structures at voltages over 50 V. Therefore, a guard ring structure was designed and fabricated (see Fig. 4) with the intent of getting avalanche before permanent breakdown. While this was not a true IMPATT design, it does show the feasibility of a Schottky based IMPATT diode. The best I-V characteristics of these guard ring Schottky diodes are shown in Fig. 15, showing relatively good rectifying characteristics out to 100 V reverse bias. However, increased voltage caused permanent breakdown of the Schottky contact, with the damage occurring inside of the guard ring. This indicates that the breakdown is not caused by the edge corona effect, but by some other mechanism, possibly related to crystal defects or surface states. Since the IMPATT modeling for a flat profile structure discussed previously indicated the need of having avalanche in an epilayer of this same carrier concentration, and no avalanche characteristics were observed, it was decided to abandon Schottky diode based IMPATTs unless the avalanche voltage could be brought down to about 50 V using a "high-low" structure.

Alternatively, 6H-SiC pn junction diodes have been fabricated that demonstrate very good avalanche breakdown characteristics at very high voltages, as shown in Fig. 16. Because of these results, further IMPATT structures were based on pn junction diodes. The initial design for SiC IMPATTs use a mesa pn junction structure with a passivated sidewall. A variety of epilayer structures were grown so that the best configuration could be determined. Both p^+-n and n^+-p flat profiles were grown, as well as the p^+-n^+-n^- high-low structure discussed above. The epilayers were all grown on n^+ substrates for maximum conductivity, and then mesas were reactive ion

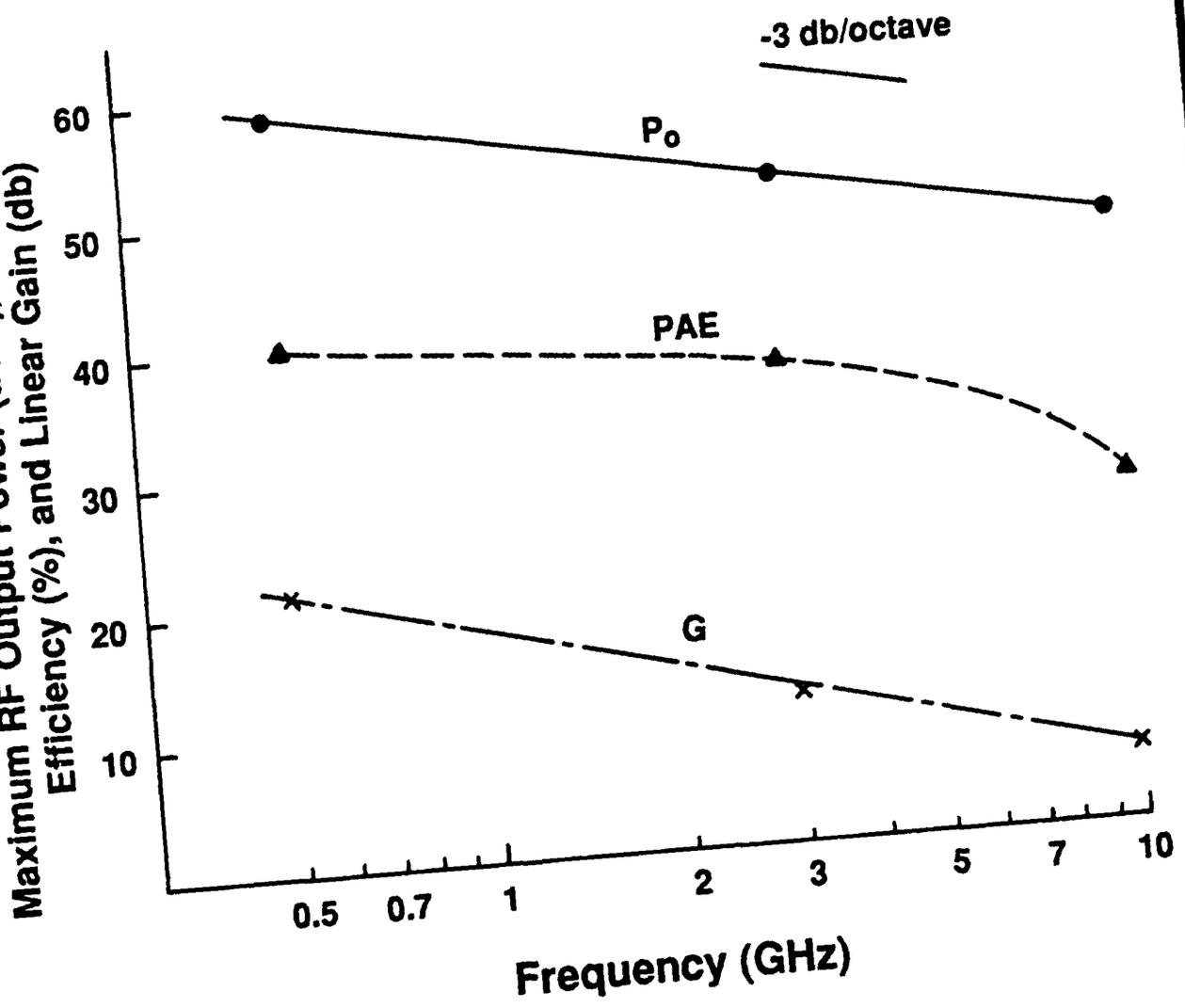

Figure 14: Modeled maximum RF performance as a function of frequency for 6H-SiC MESFETs (V_{DS} = 40 V, I_{DS} = I_{DSS}/2, L_g = 1 mm). RF output powers of 630 W, 158 W, and 45 W were obtained at 0.5, 3, and 10 GHz, respectively.

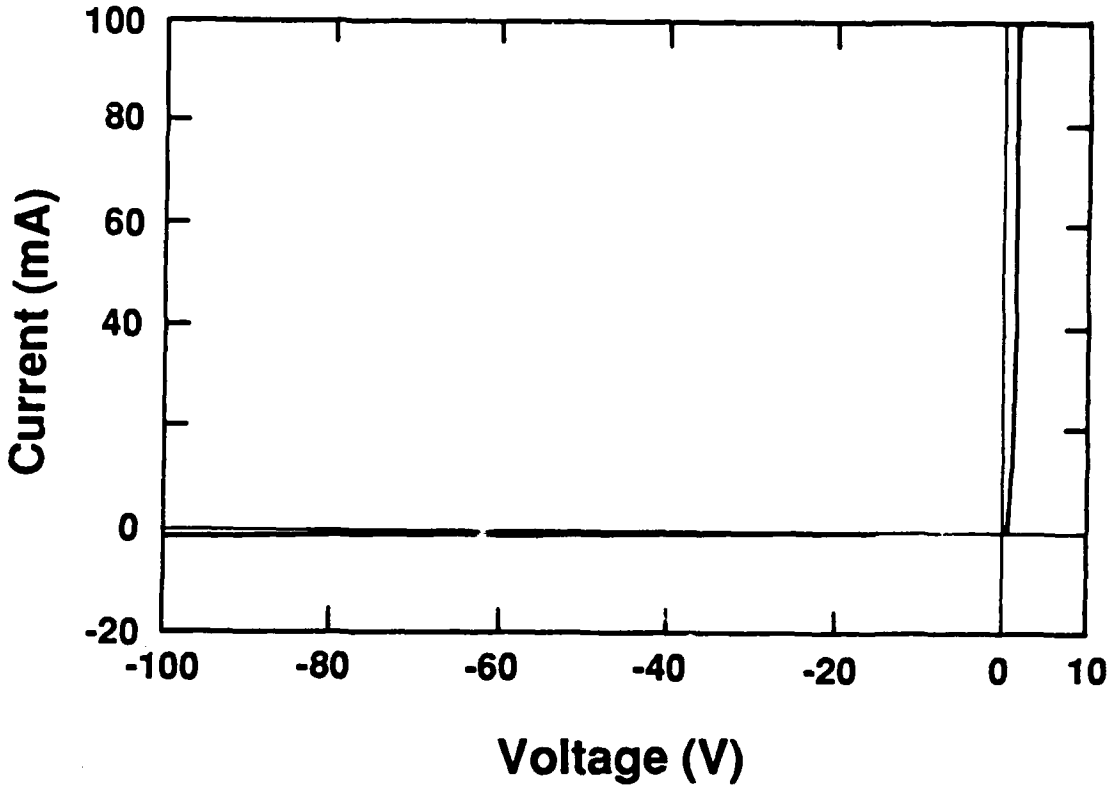

Figure 15: Current-voltage characteristics of a "guard ring" Schottky diode on n-type 6H-SiC, as shown in Fig. 4. Contact area is 4.36×10^{-3} cm^2.

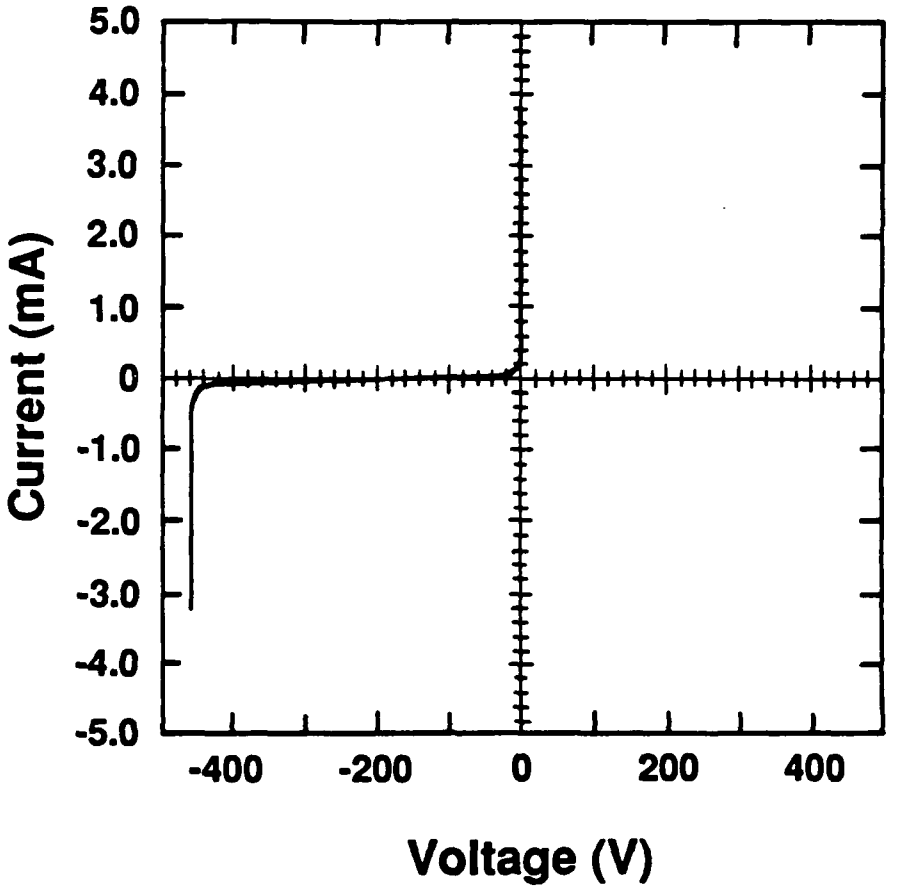

Figure 16: Current-voltage characteristics of a 6H-SiC pn junction diode, showing avalanche breakdown at 400 V.

etched in the SiC to a depth of 14 μm. The sidewalls were passivated via thermal oxidation, and the p-type ohmic contacts were defined and annealed on top of the mesas.

The original processing scheme was to then lap away the substrate from the backside until only the mesas were left. Ohmic contacts would then be deposited on the backside of these dots, and the individual mesas, or diodes would subsequently be annealed. This would result in very small discrete diode "dots" that are 14 mm thick. However, after much exp mentation it was determined that this process was difficult to perform and was not a promising technique. It is planned to finish these devices instead by lapping the wafer to a thickness of about 60-70 mm, and then depositing and patterning Al on the backside to allow reactive ion etching of contact via holes to a depth of about 40 μm. After the Al mask is stripped, the Ni ohmic contact can be deposited over the entire backside, and the wafer can be annealed. This scenario would allow the devices to be handled in wafer form instead of trying to handle very small discrete dots, but would still allow the effective substrate thickness to be very thin.

A persual of the foregoing shows that ohmic and Schottky contacts are in several cases the principal limiting aspect of making very good SiC devices. The following section describes a program which has been established to determine the proper materials and study the interface reactions at the contact-SiC interface and to relate the resulting interface chemistry to the electrical propeties of the SiC.

III. Choices of Metal Contacts to 6H-SiC

A. Introduction

As SiC becomes increasingly important for applications such as high temperature, high frequency, and high power, the need to understand the science at SiC/metal interfaces becomes crucial. Because the performance of electronic devices depends highly upon the character of contacts between semiconductors and metals, it is important to be able to choose metal contacts based on knowledge of chemistry and physics at the contact. In particular, reliable ohmic and rectifying contacts are needed. However, at this point in time, little is known about the actual chemistry and physics at interfaces between SiC and various metals.

After choosing metal contacts based on theoretical predictions, the contacts can be analyzed, and comparisons between theory and experiment can be made. This report describes the theoretical predictions and criteria on which the choices of metals have been based.

As the properties at the interface between the metal and semiconductor depends highly upon the nature of the two materials, much time has been spent considering the optimum materials for this research project. As SiC exists in hexagonal, rhombohedral, and cubic crystal structures, a hexagonal form has been chosen based on its merits at the current time. While the cubic form is referred to as b-SiC, the numerous hexagonal and rhombohedral forms are referred to collectively as a-SiC. The most common a form, 6H-SiC, has been chosen because current technology allows growth of 6H-SiC which is free of double positioning boundaries (DPB's)[4] and other defects.

B. Barrier Heights

The barrier heights of all the metals with n-type 6H-SiC have been calculated from first principles. By assuming ideal conditions (i.e. no surface states), barrier heights can be calculated easily, and theories can later be modified to explain experimental results. Since the Fermi levels of two materials which come into intimate contact must align at equilibrium, an expression for the barrier height, F_B, is the following:

$$F_B = (E_G - E_{FS}) + (F_M - F_S)$$

where E_G is the band gap of the semiconductor, E_{FS} is its Fermi level with respect to the top of its valence band, and F_M and F_S are the work functions of the metal and semiconductor respectively. The energy values for 6H-SiC have been taken from J. Pelletier, et al.[5], who have reported the

existence of Fermi level pinning. With E_G = 2.86 eV, E_{FS} = 1.443 eV, and F_S = 4.80 eV, the expression can be simplified to

$$F_B = 1.417 \text{ eV} + (F_M - 4.80 \text{ eV}).$$

Table 1 lists work functions and calculated barrier heights for most of the elements in the periodic table. Figure 17 shows these barrier heights in a graphical form.

C. Choices for Rectifying Contacts

Since n-type SiC will be used, it is desired to have a large positive barrier height. Table 2 lists the five metals with theoretical barrier heights above 2.0 eV. Selenium has the largest value, while iridium, rhenium, and platinum have values within 0.06 eV of each other.

From this list two metals have been chosen based on physical properties and economic factors. As shown in Table 2, all are high temperature materials except Se. In addition, its resistivity is five orders of magnitude higher than the other materials. However, as F. Jansen at Xerox Corp. in Webster, NY has offered to thermally evaporate Se on our samples for us and its potentially large barrier height may serve an educational purpose, we have chosen Se to study as a metal contact. As the properties listed for Ir, Re, and Pt do not differ significantly, Pt has been chosen as the second metal contact to study.

While Pt is not known to form any carbide compounds,[9] at least five silicides are known to exist (Pt_3Si, Pt_7Si_3, Pt_2Si, Pt_6Si_5, and PtSi) with the lowest eutectic at 830°C[10]. On the other hand, there is a possibility of selenium forming a carbide (CSe_2), which has a melting point of -45.4°C and a boiling point of 124°C[11]. Its silicide formation looks to be much simpler than that of Pt's; at least one silicide, $SiSe_2$ is known to exist[12].

D. Choices for Ohmic Contacts

In the hopes of forming stable ohmic contacts, metals with large negative values of theoretical barrier height have been considered first. However, a majority of elements with large negative values (Figure 1) are highly reactive, oxidize rapidly, have low melting points, and/or may contaminate active device regions. After considering these factors, three candidates with negative values were left: Sr, Sm, and Y. In addition, four candidates with positive theoretical barrier heights were added to the list based on a potential to form ohmic contacts through carbide or silicide formation. Table 3 lists the seven final candidates along with some important physical properties.

Table 1: Work functions and theoretical barrier heights to 6H-SiC.

Atomic no.	Element	Φ_M(eV)*	Φ_B(eV)
3	Li	2.9	-0.483
4	Be	4.98	1.597
5	B	4.45	1.067
6	C	5	1.617
11	Na	2.75	-0.633
12	Mg	3.66	0.277
13	Al	4.28	0.897
13	Al(100)	4.41	1.027
13	Al(110)	4.06	0.677
13	Al(111)	4.24	0.857
14	Si n	4.85	1.467
14	Si p(100)	4.91	1.527
14	Si p(111)	4.6	1.217
19	K	2.3	-1.083
20	Ca	2.87	-0.513
21	Sc	3.5	0.117
22	Ti	4.33	0.947
23	V	4.3	0.917
24	Cr	4.5	1.117
25	Mn	4.1	0.717
26	Fe	4.5	1.117
27	Co	5	1.617
28	Ni	5.15	1.767
28	Ni(100)	5.22	1.837
28	Ni(110)	5.04	1.657
28	Ni(111)	5.35	1.967
29	Cu	4.65	1.267
29	Cu(100)	4.59	1.207
29	Cu(110)	4.48	1.097
29	Cu(111)	4.94	1.557
29	Cu(112)	4.53	1.147
30	Zn	4.33	0.947
31	Ga	4.2	0.817
32	Ge	5	1.617
34	Se	5.9	2.517
37	Rb	2.16	-1.223
38	Sr	2.59	-0.793
39	Y	3.1	-0.283
40	Zr	4.05	0.667
41	Nb	4.3	0.917
41	Nb(001)	4.02	0.637
41	Nb(110)	4.87	1.487
41	Nb(111)	4.36	0.977
41	Nb(112)	4.63	1.247
41	Nb(113)	4.29	0.907
41	Nb(116)	3.95	0.567
41	Nb(310)	4.18	0.797
42	Mo	4.6	1.217
42	Mo(100)	4.53	1.147
42	Mo(110)	4.95	1.567

Atomic no.	Element	Φ_M(eV)*	Φ_B(eV)
42	Mo(111)	4.55	1.167
42	Mo(112)	4.36	0.977
42	Mo(114)	4.5	1.117
42	Mo(332)	4.55	1.167
44	Ru	4.71	1.327
45	Rh	4.98	1.597
46	Pd	5.12	1.737
47	Ag	4.26	0.877
47	Ag(100)	4.64	1.257
47	Ag(110)	4.52	1.137
47	Ag(111)	4.74	1.357
48	Cd	4.22	0.837
49	In	4.12	0.737
50	Sn	4.42	1.037
51	Sb	4.7	1.317
52	Te	4.95	1.567
55	Cs	2.14	-1.243
56	Ba	2.7	-0.683
57	La	3.5	0.117
58	Ce	2.9	-0.483
60	Nd	3.2	-0.183
62	Sm	2.7	-0.683
63	Eu	2.5	-0.883
64	Gd	3.1	-0.283
65	Tb	3	-0.383
71	Lu	3.3	-0.083
72	Hf	3.9	0.517
73	Ta	4.25	0.867
73	Ta(100)	4.15	0.767
73	Ta(110)	4.8	1.417
73	Ta(111)	4	0.617
74	W	4.55	1.167
74	W(100)	4.63	1.247
74	W(110)	5.25	1.867
74	W(111)	4.47	1.087
74	W(113)	4.18	0.797
74	W(116)	4.3	0.917
75	Re	4.96	1.577
76	Os	4.83	1.447
77	Ir	5.27	1.887
78	Pt	5.65	2.267
79	Au	5.1	1.717
79	Au(100)	5.47	2.087
79	Au(110)	5.37	1.987
79	Au(111)	5.31	1.927
80	Hg	4.49	1.107
81	Tl	3.74	0.357
82	Pb	4.25	0.867
83	Bi	4.22	0.837
90	Th	3.4	0.017
92	U	3.63	0.247

*Data taken from (3).

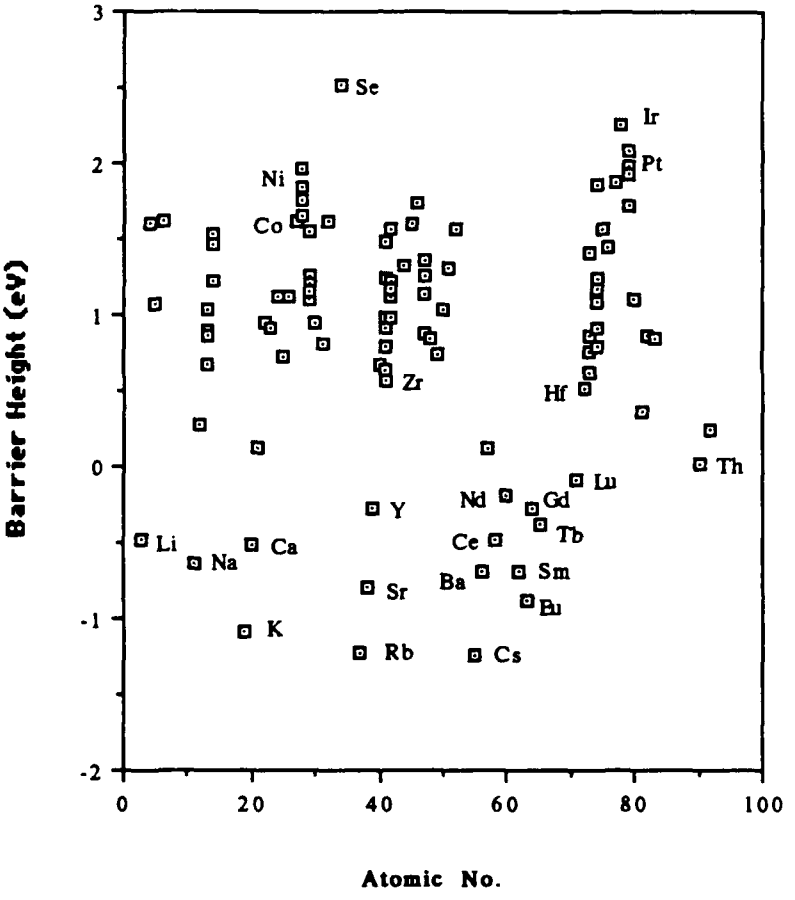

Figure 17: Theoretical barrier heights to n-type 6H-SiC

Table 2: Properties of candidates for rectifying contacts.

Element	F_B(eV)	M.P.(°C)[4]	B.P.(°C)[4]	Resistivity(mm-cm)[5]
Se	2.517	217	685	10^6
Ir	2.317	2410	4130	5.3
Re	2.367	3180	5627	19.3
Pt	2.317	1772	3827	10.6
Pd	2.217	1552	3140	10.8

Table 3: Properties of candidates for ohmic contacts.

Element	F_B(eV)	M.P.(°C)[4]	B.P.(°C)[4]	Resistivity(mm-cm)[5]
Sr	-0.793	769	1384	23
Sm	-0.693	1077	1791	88
Y	-0.283	1522	3338	57
Hf	0.517	2227	4602	35
Zr	0.667	1852	4377	40
Co	1.617	1495	2870	6
Ni	1.767	1453	2732	7

Table 4: Summary of carbide and silicide formation for ohmic contact candidates.

Element	Proposed no. of carbides	Lowest eutectic(°C)	Proposed no. of silicides	Lowest eutectic(°C)
Sr[a,c]	1	-	2	700
Sm[a,b]	3	-	3	880(?)
Y[a]	≥ 4	-	4	1215
Hf[a,b]	1	2210	5	>1300
Zr[a,c]	1	>1800	7	1360
Co[c]	0	1274	4	1195
Ni[c]	0	1318	6	964

[a]Data taken from F. Shunk (see ref. 6).
[b]Data taken from R. Elliot (see ref. 10).
[c]Data taken from M. Hansen(see ref. 9).

The combination of the information in Table 3 and phase diagrams of the metals with Si and C served to condense our list to three metals. Table 4 summarizes these phase diagrams and lists their references. Due to the very high complexity of the Y-C phase diagram, Y was excluded from the list of potential ohmic contacts.

Three other metals were eliminated based on the information in Tables 3 and 4. Hf has a lower theoretical barrier height, a slightly lower resistivity, and a higher melting point than Zr. In addition, the phase diagrams are similar, but those with Hf are slightly simpler. Therefore, Hf looks to be a better candidate than Zr. For similar reasons, Co has been chosen over Ni.

A comparison of Sr and Sm is less clear cut. While Sr is known to form one carbide (SrC_2) in comparison to Sm's three carbides, SrC_2 is proposed to go through a transformation at 370°C[14]. Since characteristics of the phase diagrams don't seem to favor either Sm or Sr, the decision was based on the theoretical barrier heights and electrical resistivities of the two metals. Table 3 shows that Sr has both a lower theoretical barrier height and a lower resistivity. Therfore Sr was chosen over Sm.

E. Future Experimental Work

As it is desired to both understand the science at metal/SiC contacts and form good, reliable contacts, the processing and analytical techniques will be important. After cleaning the surface of the SiC substrate, the surface will be studied by low energy electron diffraction (LEED). Electron beam evaporation and/or sputtering and thermal evaporation will be employed to deposit the metals.

The contacts will be analyzed for electrical, chemical, and microstructural information. Contact resistance will be studied as a function of annealing temperature and time. In addition, electrical characteristics can be quantified by I-V and C-V measurements. Chemical information may be obtained from Auger electron spectroscopy (AES), x-ray photoelectron spectroscopy (XPS), and secondary ion mass spectroscopy (SIMS). Transmission electron microscopy (TEM) will be employed to study microstructure at interfaces.

F. Conclusions

Two metals have been chosen as potential rectifying contacts to n-type 6H-SiC, while there are still three candidates for potential ohmic contacts. Platinum and Se were chosen for rectifying contacts based on their high theoretical barrier heights. Sr, Hf, and Co may be deposited in the

hopes of finding good, reliable ohmic contacts. These three metals were chosen based on the merits of their theoretical barrier heights, physical properties, and phase diagrams with Si and C.

Although the five metals have been chosen based on theoretical predictions and physical properties, there are still some physical properties, such as thermal expansion coefficients, which need to be studied more carefully. Therefore, it is possible that a metal may be added to or excluded from the list at a later date.

IV. MOLECULAR BEAM EPITAXY OF SILICON CARBIDE

A. Introduction

A system for the growth of SiC films by the technique of gas-source molecule beam epitaxy has been designed, purchased, and is currently under construction. The technique of molecular beam epitaxy (MBE) allows for precise control of growth parameters and minimization of sample contamination. Monocrystalline SiC films will be grown at relatively low temperatures using minute amounts of gas introduced into the system by leak valves. Pressures within the chamber during growth will be in the 10^{-5} torr range. As the mean free path of molecules at this pressure is much longer than the dimensions of the growth chamber, the source gas molecules reach the sample surface without collisions. Thus a great deal of control over growth conditions can be achieved using this technique. This deposition system will be used for low defect-density growth of monocrystalline SiC thin films, SiC/AlN solid solutions , and SiC/AlN pseudomorphic structures.

B. Growth System

A schematic of the system is shown in figure 18. Samples will be introduced into a small load lock chamber, which will be subsequently evacuated. The samples will then be transferred to the heating stage in the growth chamber. The load lock is used in order to increase sample throughput, as well as to keep the main deposition chamber under vacuum. It is pumped by a turbomolecular pump backed by a rotary vane pump. The load lock is fully constructed, and pressures of 1×10^{-6} torr or below are reached within 30 minutes after pumping begins.

The growth chamber will be utilized for both *in situ* sample cleaning and deposition. Substrates will be cleaned prior to deposition by using Ar plasma to produce H^+ radicals from H_2 introduced into the system downstream from the plasma. The Ar plasma will be obtained using an electron cyclotron resonance plasma source developed in our laboratory by Sitar. This source should be completed within two months. To date, no published work has been performed on plasma cleaning of α-SiC. However H^+ plasma cleaning of silicon using this method has been performed at 300°C [15].

The growth chamber has been designed to maximize versatility and minimize sample contamination. It has the capability of using gaseous sources introduced into the chamber using automatic variable control leak valves. The leak rates can be varied precisely and automatically as a function of time, or flow can quickly be shut off and on using solenoid valves. As a result,

Schematic Diagram of Gas-Source MBE Chamber

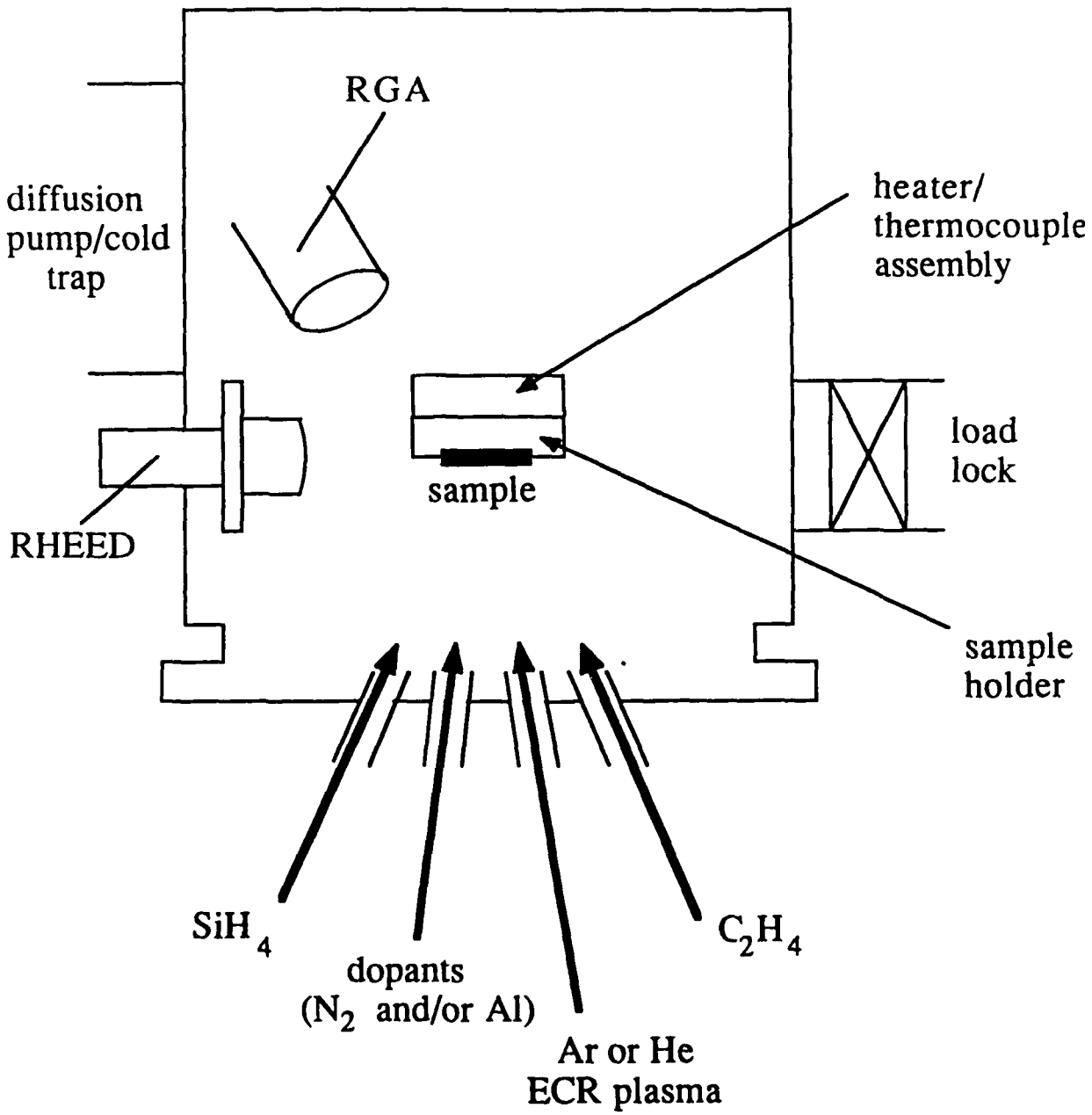

Figure 18: Schematic of molecular beam deposition system for growing SiC thin films

growth species can be reproducibly controlled. This is necessary for the growth of novel structures, such as the SiC/AAIN layered structures. Solid MBE sources (either Knudsen cells or electron-beam sources) can also be installed along the source flange and used as desired.

The electron cyclotron resonance (ECR) source used for H^+ plasma cleaning will also be used for the production of activated nitrogen species from N_2 for n-type doping of SiC. During cleaning and deposition, the sample sits at a 45° tilt from upside down in order to avoid contamination on itself from falling particulates as well as to avoid contamination of the solid sources from falling particulates generated on the sample holder and/or sample. The chamber will also have equipment for residual gas analysis in order to determine species present in the chamber during growth. Characterization of films using RHEED during growth is planned, but this equipment has yet to be purchased. The system will be pumped using a 2400 l/s diffusion pump with a Vacuum Generators UHV liquid nitrogen cold trap backed by a rotary vane pump. Background pressures of 10^{-10} torr are expected in this system. All components of this system mentioned above are either on order or have been received.

Samples will be heated using a heater specially designed for this system. Exposure of the sample to materials containing electrically active impurities, such aluminum, has been minimized. All components in contact with the sample will be high purity SiC-coated graphite. Heat is produced by resistive heating of a coiled tungsten filament within a SiC-coated graphite cylindrical heating cavity lined with tungsten heat shielding. A high-purity pyrolitic BN disk is used as an insulating plate for holding the W coil. The heater will be capable of temperatures of well over 1000°C, which is necessary for this research.

C. Experimental Details

Low temperature growth of high-purity, low defect-density, monocrystalline SiC layers on α-SiC substrates is the primary goal of this project. These SiC films will be grown on α-SiC substrates obtained from Cree Research. Gases initially to be used for growth of SiC are silane (SiH_4) as the Si source and ethylene (C_2H_4) for the carbon source. An emphasis has been placed on finding a solid carbon source for the production of monomolecular carbon species, as decomposition of hydrocarbons requires fairly high temperatures. The growth temperature of SiC can be substantially lowered if the energy required for this decomposition can be decreased. Plasma decomposition is a proven method for low-temperature decomposition of gaseous species, though the process control necessary for monocrystalline growth is not easily achieved.

The feasibility of a heated graphite filament for carbon doping of GaAs in a MBE system has recently been demonstrated[16]. A large percentage of monomolecular C has been produced by resistive heating of graphite to temperatures of about 2500°C. This carbon source is very simple and effective and has potential as a solid source for carbon in SiC. Though the carbon flux from the graphite filament must be much greater for SiC than for doping of GaAs, the use of a filament with a larger cross-section and greater power should give a sufficiently large carbon flux. Other methods of producing a flux of C, such as modified electron beam evaporation to produce monomolecular species, are also being considered. Dopants to be used for SiC are Al (p-type) obtained by thermal decomposition of triethylamuminum(TEA) and N obtained by the Decomposition of N_2 using the ECR source noted above. Growth temperatures will be in the range of 1000-1200°C.

In addition to SiC films, SiC/AIN pseudomorphic layers and solid solutions will also be grown as a part of this research. Research conducted in the U.S. and the Soviet Union indicates that a wide range of solid solutions exists in the SiC/AIN system. A solid solution between these materials would undoubtedly have interesting electrical properties, such as the effective bandgap as a function of AlN in the solid solution.

In addition, the lattices of the hexagonal polytypes of SiC and AIN have an effective mismatch in the axial direction of less than 1%. Layers of these materials below a certain thickness will elastically strain to accommodate each other. If the layers are monocrystalline, this will produce a pseudomorphic structure. This structure will undoubtedly have novel properties. For example, a pseudomorphic structure with SiC (an indirect bandgap material) and AIN (a direct bandgap material) may have a direct bandgap intermediate between the two materials. The same could be true of a SiC/AIN solid solution in certain composition ranges. These structures may prove to have many useful applications. Experimental work to produce these novel structures and examine their effects on material properties will take place in future research.

ACKNOWLEDGEMENTS

The high frequency modeling work described in Section II was partially funded by Westinghouse Electric Corporation, Defense and Electronics Center.

REFERENCES

1. S. Yoshida, K. Sasaki, E. Sakuma, S. Misawa, and S. Gonda, Appl. Phys. Lett. **46**, 766 (1985).

2. H. S. Kong, J. W. Palmour, J. T. Glass, and R. F. Davis, Appl. Phys. Lett. **51**, 442 (1987).

3. N. A. Papanicolaou and A. Christou, "Abstracts of the Fourth National SiC Review Meeting," at N. C. State University (Oct. 26 - 27, 1987).

4. H.S. Kong, J.T. Glass, and R.F. Davis, J. Appl. Phys. **64**(5), 2672 (1988).

5. J. Pelletier, D. Gervais, and C. Pomot, J. Appl. Phys. 55(4), 994 (1984).

6. **CRC Handbook of Chemistry and Physics**, Ed. R. Weast (CRC Press, Inc., Boca Raton, FL, 1989), p. E-93.

7. **CRC Handbook of Chemistry and Physics**, Ed. R. Weast (CRC Press, Inc., Boca Raton, FL, 1979), p. D-190.

8. Ibid., p.F-171.

9. F. Shunk, **Constitution of Binary Alloys**, (McGraw-Hill Book Co., New York, 1969), p. 153.

10. Ibid., p. 623.

11. Ibid., P. 156.

12. M. Hansen, Constitution of Binary Alloys, (McGraw-Hill Book Co., New York, 1958), p.1186.

13. R. Elliot, **Constitution of Binary Alloys**, (McGraw-Hill Book Co., New York, 1965).

14. M. Hansen, Ibid., p. 380.

15. R. Rudder, G. Fountain, and R. Markunas, J. Appl. Phys. **60**, 3519 (1986).

16. R.J. Malik, R.N. Nottenberg, E.F. Schubert, J.F. Walker, and R.W. Ryan, Appl. Phys. Lett. 53, 2661 (1988).

Distribution List

Name/Address	No. of Copies
Dr. Yoon Soo Park Office of Naval Research, Code: 1212 Applied Research Division 800 North Quincy Street Arlington, VA 22217-5000	2
Ms. Marta Morris ONR Resident Representative Office of Naval Research 1314 Kinnear Road Columbus, OH 43212-1104	2
Director, Naval Research Laboratory ATTN: Code - 2627 Washington, DC 20375	7
Defense Technical Information Center Building 5 Cameron Station Alexandria, VA 22314	14
Dr. Calvin Carter, Jr. Dr. John Palmour Cree Research 2810 Meridian Parkway Suite 176 Durham, NC 27713	2